An updated force balance approach to investigate bubble sliding in vertical flow boiling at low and high pressures

L. Favre, Catherine Colin, S. Pujet, S. Mimouni

An updated force balance approach to investigate bubble sliding in vertical flow boiling at low and high pressures

L. Favre[1,2,*], C. Colin[2], S. Pujet[1], S. Mimouni[1]

Abstract

An analysis of bubble sliding in vertical flow boiling is conducted using a reworked force balance including a recent formulation of the drag coefficient along with a proper derivation of added mass coefficients. The modeling strategy was further performed to avoid the use of too many empirical parameters.

This offers the possibility to develop a non-dimensional approach that exhibits physical ranges of dominance for the detaching forces. Applied to experimental measurements, it shows that the main forces triggering departure by sliding at low and high pressures are respectively Added Mass and Drag forces. Predictions of bubble departure diameter using the force balance achieves good agreement over 122 measurements from several experimental data sets.

Bubble sliding measurements from the literature at low and high pressures permitted to validate the model which was able to predict bubble velocity provided the use of a correct bubble growth rate.

Keywords: Vertical Flow Boiling, Bubble Departure Diameter, Bubble Sliding, Force Balance, Mechanistic Model, Non-Dimensional Approach

Nomenclature

Acronyms

BC	Boiling Crisis
CHF	Critical Heat Flux
DNS	Direct Numerical Simulations
HFP	Heat Flux Partitioning
PWR	Pressurized Water Reactor

*First corresponding author, favre.luc05@gmail.com

[1]Électricité de France Recherche & Développement (EDF R&D), 6 Quai Watier, Chatou, 78400, France

[2]Institut de Mécanique des Fluides de Toulouse (IMFT), Université de Toulouse, CNRS/INPT/UPS, Allée Camille Soula, Toulouse, 31400, France

RPE Rayleigh-Plesset Equation

SMR Small Modular Reactor

Greek symbols

η Thermal diffusivity[m^2/s]

γ Shear rate [s^{-1}]

λ Thermal conductivity [W/m/K]

μ Dynamic viscosity [$J.s/m^{-3}$]

ν Kinematic viscosity [m^2/s]

ϕ Heat flux [$J/m^2/s$]

ρ Density [kg/m^3]

σ Surface tension [J/m^2]

θ, $d\theta$ Contact angle and half-hysteresis [° or rad]

θ_i Bubble inclination angle [° or rad]

Latin symbols

C Force coefficient [-]

D Bubble diameter [m]

D_h Hydraulic diameter [m]

E Kinetic energy [J]

F Force [N]

G Mass flux [$kg/m^2/s$]

g Gravity acceleration [m^2/s]

h_{LV} Latent heat of vaporization [J/kg]

K Bubble growth constant [-]

$L_c = \sqrt{\frac{\sigma}{(\rho_L - \rho_V)g}}$ Capillary length [m]

l_{sl} Bubble sliding length [m]

R Bubble radius [m]

R_c Bubble curvature radius [m]

r_w Bubble foot radius [m]

T Temperature [K]

U Velocity [m/s]

U_τ Wall friction velocity [m/s]

$U_{rel} = U_L - U_b$ Relative velocity [m/s]

V Volume [m^3]

Non-dimensional numbers

$\mathrm{Ca} = \frac{\mu_L U_L}{\sigma}$ Capillary number [-]

$\mathrm{Eo} = \frac{(\rho_L - \rho_V)gR^2}{\sigma}$ Eotvos number [-]

$\mathrm{Fr} = \frac{\rho_L U_L^2}{(\rho_L - \rho_V)gR}$ Froude number [-]

$\mathrm{Ja} = \frac{\rho_L c_{P,L}|T - T_{sat}|}{\rho_V h_{LV}}$ Jakob number [-]

$\mathrm{Pr} = \frac{\nu}{\eta}$ Prandtl number [-]

$\mathrm{Re}_b = \frac{U_{rel} D_b}{\nu_L}$ Bubble Reynolds number [-]

$\mathrm{Re}_{D_h} = \frac{G_L D_h}{\mu_L}$ Liquid bulk Reynolds number [-]

$\mathrm{Sr} = \frac{2\gamma R}{|U_{rel}|}$ Non-dimensional shear rate [-]

$y^+ = \frac{y U_\tau}{\nu_L}$ Non-dimensional wall distance [-]

Subscripts

AM Added-Mass

b Bubble

D Drag

d Departure or Downstream

L Lift or Liquid

lo Lift-off

sat	Saturation	V	Vapor
u	upstream	w	Wall

1. Introduction

Studying the local physics of boiling two-phase flows has been a primal field of research for decades both due to its intrinsically complicated nature and its huge importance for many industrial fields such as:

- Nuclear Pressurized Water Reactors (PWR) ;
- Small Modular Reactors (SMR) passive cooling systems ;
- Two-phase flow loops for electronic devices cooling systems including space applications (*e.g.* satellites).

This has led to many approaches to investigate and model wall boiling in multiphase flows. Notably, Computational Multi-Fluid Dynamics codes mostly rely on a so-called Heat Flux Partitioning (HFP) model [1] which goal is to split the applied wall heat flux between different physical heat transfer phenomena (Eq. 1) such as liquid convection (c, L), phase-change (vap), transient conduction (tc), etc.

$$\phi_w = \phi_{c,L} + \phi_{tc} + \phi_{vap} \tag{1}$$

Many HFP models have been developed over the years, starting with Kurul & Podowski [2] who validated their model against vertical flow boiling measurements. Later, Basu *et al.* [3] developed a model including bubble sliding and renewed closure laws based on their own experimental results of vertical flow boiling at low pressure and mass fluxes. More recently, Gilman & Baglietto [4] also proposed new formulations for the HFP compared with measurements in vertical flow boiling of water. Those models constitute pivotal elements for bubble dynamics in multiphase flows simulations and are often under scrutiny as performed by Bhati *et al.* [5] who studied axial evolution of boiling parameters in a vertical channel.

Upgrades of HFP models always aim to consider new heat transfer mechanisms or better closure laws for parameters like Nucleation Site Density or Bubble Departure Frequency or Diameter. Among those models, bubble dynamics is of prior interest for predicting bubble departure diameter, sliding length, and lift-off diameter. Those parameters play a significant role in the estimation of the transient conduction heat flux ϕ_{tc} and boiling heat flux ϕ_{vap}. Since transient conduction is associated to bubble

movement disrupting the liquid boundary layer, it is directly depending on the value of the bubble diameter and its sliding length.

Many experimental investigations have been conducted to further understand the behavior of nucleated bubbles in boiling flows. In the case of vertical flow boiling, a sliding phase during which the bubble remains attached to the wall is quasi-systematically observed both at low pressure [6, 7, 8] and high pressure [9]. The bubble sliding process has also been thermally studied by Estrada-Perez *et al.* [10] who observed the significant impact of sliding bubbles footprints on the heat flux. Richenderfer *et al.* [11] and Kossolapov [9] have also investigated the sliding of boiling bubbles and measured the magnitude of the transient heat transfer induced by the disruption of the liquid thermal boundary layer in the bubble's wake.

Thus, it appears important to properly model boiling bubbles dynamics to distinguish the different phases of the bubble lifetime:

- Static growth on the wall before departure by sliding at radius R_d ;
- Sliding on the wall over a length l_{sl} before lifting off towards the bulk flow at radius R_{lo}.

First approaches consisted of experimental-based correlations. For instance, we can refer to the work of Unal [12] or Situ *et al.* [6] for the lift-off / maximum bubble diameter D_{lo}, to Maity [7] or Basu *et al.* [3] for the sliding length l_{sl} and to Klausner *et al.* [13], Maity [7] or more recently Zhou *et al.* [14] for the departure diameter D_d. Those models mostly rely either on pure data regression or semi-analytic approaches.

However, explicit correlations include limited range of application depending on the flow conditions over which they have been established. To overcome this drawback and to obtain more generalized models, researchers have developed Mechanistic Models based on a force-balance approach to depict the external efforts experienced by the growing bubble. The goal is to compute the sum of the forces applied to the bubble over its growing time and to detect departure and lift-off events using criteria such as a change in the force balance sign.

One of the firstly introduced model was proposed by Klausner *et al.* in 1993 [13] validated on horizontal flow boiling of refrigerant. It was followed by several subsequent works among which Van Helden *et al.* [15] who assessed forces coefficients using injected air bubbled in a vertical flow or Thorncroft [16] who compared his predictions with vertical and horizontal flow boiling of R113. Later, Duhar & Colin [17] validated a force balance on bubbles created by air injection in a shear flow. Sugrue *et al.* [18] studied water flow boiling with varying surface orientation with their results used by Mazzocco *et al.* [19] who validated his model against several

low pressure measurements from literature. For more recent works, we can mention Ren *et al.* [20] who used own measurements of vertical flow boiling of water up to 5 bar or Bhati & Paruya [21] who numerically investigated bubble growth, shape and departure in pool boiling. Each of those models proposed different modifications to the force balance depending on the aimed experimental conditions.

Unfortunately, all the aforementioned works were validated using low pressure experiments due to the lack of pressurized measurements in the literature. In addition, the common use of several empirical parameters makes it difficult to reach a general validation of those models. The present study, anchored in this framework, aims to propose an update of the bubble force balance for vertical boiling flows with a reduced empiricism and to study the sliding phenomenon by conducting a non-dimensional analysis of the departure by sliding as well as predicting the subsequent departure diameter and sliding velocity of the bubble. By focusing on the force balance parallel to the wall, the approach is validated against measurements in various flow conditions, including pressures up to 40 bar thanks to the recent work of Kossolapov [9]. This ensures an encouraging generality of the proposed approach compared to previous models.

2. Force Balance Modeling

2.1. General Considerations

When trying to derive the force balance over a bubble, the first step consists of splitting the whole effort experienced by the bubble between different contributions depending on their nature. In our case, we focus on a bubble growing on a vertical wall and facing an upward flow as depicted in Figure 1.

The static forces are:

- The Buoyancy force $\overline{F_B}$, including Archimedes force and the weight of the bubble ;
- The Capillary or Surface Tension force $\overline{F_C}$;
- The Contact Pressure force $\overline{F_{CP}}$.

The hydrodynamic forces are:

- The Drag and Lift forces $\overline{F_D}$ and $\overline{F_L}$;
- The Inertia force, including Added-Mass and Tchen force $\overline{F_I}$.

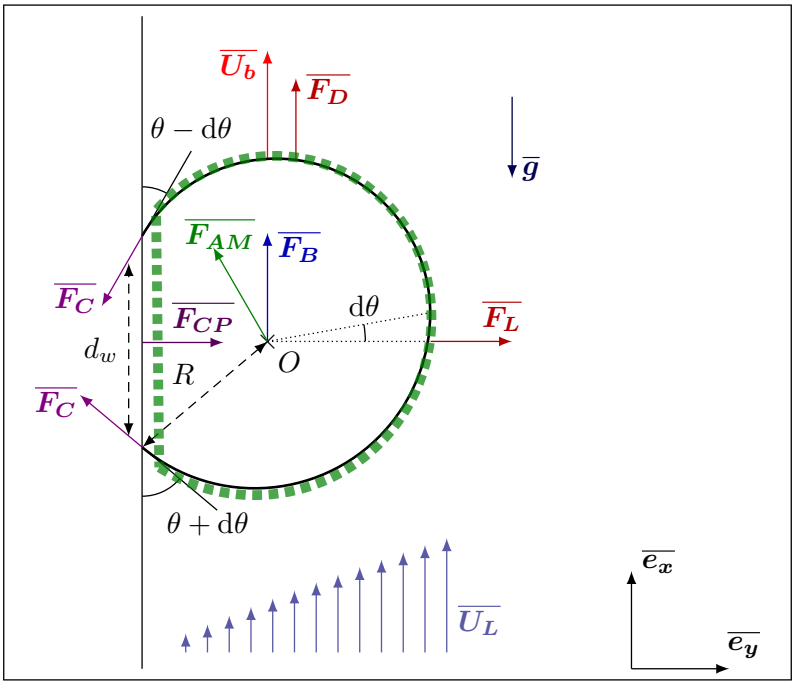

Figure 1: Sketch of the forces applied to the bubble facing an upward flow $\overline{U_L}$ and sliding at velocity $\overline{U_b}$. Green dashed lines show the control volume for the force balance, excluding the microlayer or microregion.

Regarding the bubble shape, we consider a quasi-spherical bubble of radius R with a circular base of radius r_w. Depending on the experimental conditions (fluid wettability, pressure, heat flux, liquid temperature), a liquid microlayer can be formed between the wall and the vapor bubble. It occurs when the bubble growth velocity is larger than the dewetting velocity of the liquid on the wall [22]. Recent experiments of Kossolapov [9] have shown that this microlayer also exists in vertical flow boiling of water at atmospheric pressure, but disappears at pressures larger than 3 bars. In the present analysis microlayer may be present or not. In case of a microlayer, the bubble base is taken above the microlayer. The control volume used for the evaluation of the force balance is plotted in dashed line in Figure 1. The contact angles on both sides of the bubble are macroscopic contact angles outside the microregion or the microlayer. The resulting downstream (receding) and upstream (advancing) contact angles are $\theta_d = \theta - \mathrm{d}\theta$ and $\theta_u = \theta + \mathrm{d}\theta$. If the bubble has a shape close to a truncated sphere, we can approximate the bubble foot radius as:

$$r_w \approx R \sin\left(\frac{\theta_u + \theta_d}{2}\right) = R \sin(\theta) \tag{2}$$

The choice of using the average contact angle θ instead of the average of $R\sin(\theta_u)$ and $R\sin(\theta_d)$ avoids to have $r_w \to 0$ when $\mathrm{d}\theta \to 90°$. We suppose $V_b \approx \frac{4}{3}\pi R^3$ for the bubble volume.

2.2. Buoyancy Force

The Buoyancy force results from the weight of the bubble and the integration of the static liquid pressure over its surface which naturally yields:

$$\overline{F_B} = V_b\,(\rho_V - \rho_L)\,\overline{g} = \frac{4}{3}\pi R^3\,(\rho_L - \rho_V)\,g\;\overline{e_x} \tag{3}$$

2.3. Capillary Force

The most generally accepted expression of the Capillary force has been derived by Klausner *et al.* [13] by integrating the tangential effort at the triple contact line over the bubble foot radius while assuming an evolution of the contact angle from θ_d to θ_u as a polynomial expression of degree 3. This results in:

$$\begin{aligned}\overline{F_C} = &-\pi R\sigma\left[2.5\,\frac{r_w}{R}\frac{\mathrm{d}\theta}{\left(\frac{\pi}{2}\right)^2 - \mathrm{d}\theta^2}\sin(\theta)\cos(\mathrm{d}\theta)\right]\overline{e_x}\\ &-\pi R\sigma\left[2\,\frac{r_w}{R}\sin(\theta)\,\frac{\sin(\mathrm{d}\theta)}{\mathrm{d}\theta}\right]\overline{e_y}\end{aligned} \tag{4}$$

2.4. Contact Pressure Force

The Contact Pressure force is linked to the overpressure inside the bubble. Combined with the Archimedes force, it can be expressed versus the difference of liquid and vapor pressure at the bubble foot using Laplace's equation as:

$$\overline{F_{CP}} \approx \frac{2\sigma}{R_c}\pi r_w^2\;\overline{e_y} \approx \pi R\sigma\;2\,\sin(\theta)^2\;\overline{e_y} \tag{5}$$

Here, R_c is the curvature radius of the bubble which is often assumed to be equal to $5R$ [13, 23, 19] without other explanation than avoiding an overestimation of the Contact Pressure force.

2.5. Drag and Lift Forces

The external liquid flow over the bubble induces the well-known Drag and Lift forces, acting respectively in the flow direction and perpendicular to the flow. They are usually expressed using associated coefficients C_D and C_L defined by:

$$\overline{F_D} = \frac{1}{2} C_D \rho_L S_p \left|\left|\overline{U_L} - \overline{U_b}\right|\right| \left(\overline{U_L} - \overline{U_b}\right) \tag{6}$$

$$\overline{F_L} = \frac{1}{2} C_L \rho_L S_p \left|\left|\overline{U_L} - \overline{U_b}\right|\right|^2 \ \overline{e_y} \tag{7}$$

with $S_p = \pi R^2$ the projected area of the bubble in the direction of the flow.

Traditional approaches rely on expressions of the Drag force for a bubble in an infinite medium based on numerical correlations as proposed by Mei & Klausner [24]:

$$C_{D,U} = \frac{16}{\mathrm{Re}_b} \left[1 + \left(\frac{8}{\mathrm{Re}_b} + \frac{1}{2}\left(1 + \frac{3.315}{\sqrt{\mathrm{Re}_b}}\right)\right)^{-1}\right] \tag{8}$$

with $\mathrm{Re}_b = \frac{|U_{rel}(R)|\ 2R}{\nu_L}$ the bubble Reynolds number and $U_{rel}(R) = U_L(R) - U_b$ the local relative velocity.

Results from DNS conducted by Legendre *et al.* [25] proposed expressions of the Drag and Lift forces for a hemispherical bubble on a wall facing a viscous shear flow. Earlier, Legendre & Magnaudet [25] analytically derived coefficients to transpose Drag and Lift expressions for a particle to the case of a bubble. This was applied by Mazzocco *et al.* [19] to the Drag for a solid particle near a wall in a shear flow proposed by Zeng *et al.* [26].

In this work, we propose to rely on the recent work of Shi *et al.* [27] who conducted DNS of a shear flow over a spherical bubble of constant radius close to a wall for bubble Reynolds number between 10^{-1} and 10^3 and shear rates between -0.5 and 0.5.

They computed the resulting Drag and Lift coefficients for each simulations and proposed correlations fitting their numerical results. The total Drag coefficient is expressed as a correction of the Drag coefficient for a bubble in an unbounded uniform flow $C_{D,U}$. The total drag is given by:

$$C_D = (1 + \Delta C_D)\, C_{D,U} \tag{9}$$

where ΔC_D accounts for both the effect of the shear flow and the wall vicinity.

To cover the whole range of bubble Reynolds numbers, correlations at low and high Re_b are smoothly connected using an exponential term.

$$\Delta C_D = \Delta C_{D,\mathrm{Re}_b = O(1)} + \left(1 - e^{-0.07\mathrm{Re}_b}\right) \Delta C_{D,\mathrm{Re}_b \gg 1} \tag{10}$$

Each of those corrections is computed depending on Re_b, the non-dimensional shear rate Sr, the non dimensional wall distance $L_R = \frac{y}{R}$ ($L_R = 1$ being a spherical bubble laying on a wall) and non-dimensional viscous (or Stokes) length $L_u = \frac{y}{\nu_L/|U_{rel}|}$.

$$\begin{aligned}\Delta C_{D,\mathrm{Re}_b=O(1)} =& \frac{1+\tanh\left(0.012\mathrm{Re}_b^{0.8}\right)+\tanh\left(0.07\mathrm{Re}_b^{0.8}\right)^2}{1+0.16L_u\left(L_u+4\right)} \\ &\times\left[\left(\frac{3}{8}L_R^{-1}+\frac{3}{64}L_R^{-4}\right)\left(1-\frac{3}{8}L_R^{-1}-\frac{3}{64}L_R^{-4}\right)^{-1}\right. \\ &\left.-\frac{1}{16}\left(L_R^{-2}+\frac{3}{8}L_R^{-3}\right)\mathrm{Sr}\right] \end{aligned} \tag{11}$$

$$\begin{aligned}\Delta C_{D,\mathrm{Re}_b\gg 1} =& \ 0.47L_R^{-4}+0.0055L_R^{-6}\mathrm{Re}_b^{3/4}+0.002\left|\mathrm{Sr}\right|^{1.9}\mathrm{Re}_b \\ &+0.05L_R^{-7/2}\mathrm{Sr}\mathrm{Re}_b^{1/3}\end{aligned} \tag{12}$$

Figure 2 shows the evolution of the Drag correction ΔC_D against the bubble Reynolds number for different distances to the wall L_R and two values of Sr. We can see that as the distance between the wall and the bubble increases the Drag correction logically approaches zero and that increasing the shear rate Sr increases ΔC_D for higher values of Re_b.

Shi *et al.* [27] conducted DNS for wall distances down to $L_R = 1.5$. However, Scheiff *et al.* [28] compared the values obtained for $L_R = 1$ with measured Drag coefficients of bubbles sliding on a wall and observed a good agreement, which legitimates the use of this new Drag correlation by extending its application to the case of a bubble laying on a wall and using the uniform drag coefficient of Eq. 8.

Since this work focuses on the bubble sliding along the wall, the total force balance will be studied along the x axis, parallel to the wall. Thus, we do not detail the whole expression of Shi *et al.* for the lift coefficient C_L and refer the reader to their original work [27].

2.6. Inertia Force

The Inertia force originates from various effects (bubble growth, freestream and bubble acceleration, etc.) that includes both Added Mass and Tchen forces and is expressed as [29]:

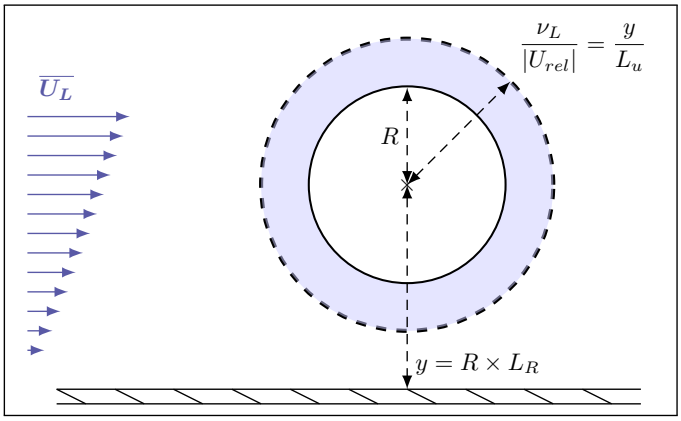

(a) Sketch of the case simulated by Shi *et al.*

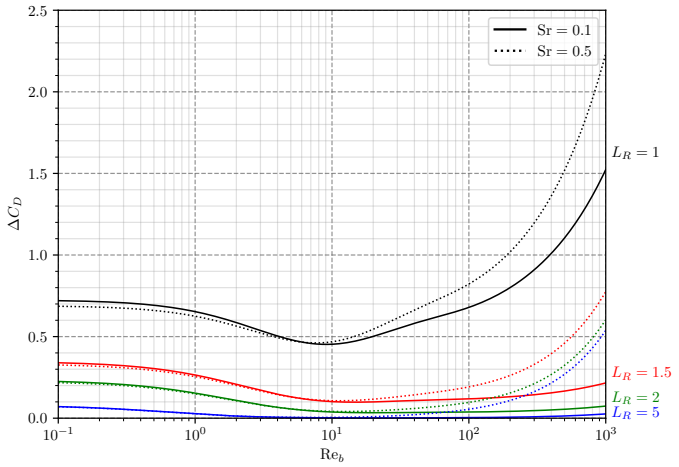

(b) Drag correction from Shi *et al.* (Eq. 10)

Figure 2: Details on the work of Shi *et al.* [27] regarding the drag correction.

$$\overline{F_I} = \underbrace{\rho_L V_b \left(\frac{\partial \overline{U_L}}{\partial t} + \overline{\overline{\nabla}} \left(\overline{U_L} \right) \cdot \overline{U_L} \right)}_{\text{Liquid inertia or Tchen force}} + \underbrace{\frac{\mathrm{d}}{\mathrm{d}t} \left(\rho_L C_{AM} V_b \left(\overline{U_L} - \overline{U_b} \right) \right)}_{\text{Added Mass force } \overline{F_{AM}}} \tag{13}$$

Since we consider a steady and quasi-parallel liquid flow, the Tchen force is equal to zero.

2.6.1. Former Approaches

In previous Mechanistic Models, the derivation of the Added Mass force was conducted with different approaches. In particular, some authors chose to rely on the Rayleigh-Plesset Equation for a growing hemispherical bubble in a quiescent flow, obtaining a reaction force from the liquid perpendicularly to the wall.

$$\overline{F_{AM,RPE}} = -\rho_L \pi R^2 \left[R\ddot{R} + \frac{3}{2}\dot{R}^2 \right] \overline{e_y} \tag{14}$$

Then, assuming a bubble inclination angle θ_i, this force was projected along the x axis to obtain an Added Mass force parallel to the wall that hinders departure. The inclination angle value is often empiricial and used for data fitting [13, 23, 19, 20].

$$\overline{F_{AM,RPE}} = -\rho_L \pi R^2 \left[R\ddot{R} + \frac{3}{2}\dot{R}^2 \right] \left(\sin\left(\theta_i\right) \overline{e_x} + \cos\left(\theta_i\right) \overline{e_y} \right) \tag{15}$$

This approach is questionable on different aspects. First, the RPE assumes a spherical symmetry and moving boundary in a quiescent unbounded liquid, which is physically far from the real situation of a bubble growing on a wall in a boiling flow. Moreover, the subsequent projection along the different directions regarding an unknown angle is hardly reasonable if θ_i is chosen arbitrarily.

On the other hand, some authors [13, 16, 30] considered two distinct contributions:

- RPE equation and inclination θ_i, leading to Eq. 15 ;
- Spherical bubble growth in an uniform unbounded and inviscid liquid flow, which yields a detaching Added Mass term due to the interaction of bubble growth with the external flow:

$$\overline{F_{AM,U}} = \frac{3}{2}\rho_L V_b \frac{\dot{R}}{R} U_L \overline{e_x} \tag{16}$$

By including the effect of the liquid flow, this approach can be considered as closer to the reality. However, it relies on two separate derivations associated to different physical considerations.

2.6.2. Proposed Approach

To tackle the Added Mass force derivation, we propose to follow the approach of Lamb [31] (also presented by Van Winjgaarden [32]). By solving the potential flow around a bubble and its image, we can obtain the total liquid kinetic energy

E_L that corresponds to a situation where a bubble is at a given distance from a wall (represented by the line normal to the line of centers of the bubbles).

Then, using Lagrange's equations to compute the resulting forces along x and y:

$$F_{AM,x} = -\frac{\partial}{\partial t}\left(\frac{\partial E_L}{\partial \dot{x}}\right) + \frac{\partial E_L}{\partial x} \tag{17}$$

$$F_{AM,y} = -\frac{\partial}{\partial t}\left(\frac{\partial E_L}{\partial \dot{y}}\right) + \frac{\partial E_L}{\partial y} \tag{18}$$

To express the liquid kinetic energy, we can rely on the work of Van Der Geld [33] who derived E_L in the case of a full or truncated growing spherical bubble laying on a wall and facing a uniform flow parallel to the wall of velocity U_L (Eq. 19). If the bubble slides at a velocity $U_b = \dot{x}$, it sees a liquid velocity $U_{rel} = U_L - \dot{x}$.

$$E_L = \frac{\rho_L V_b}{2}\left(\alpha \dot{y}^2 + \mathrm{tr}\,(\beta)\,\dot{R}^2 + \psi \dot{R}\dot{y} + \alpha_2\,(U_L - \dot{x})^2\right) \tag{19}$$

where (x, y) are the coordinates of the bubble's center and α, $\mathrm{tr}\,(\beta)$, ψ, α_2 are polynomials of $R/y = 1/L_R$ derived by Van Der Geld for $1 < R/y < 2$ *i.e.* $0.5 < L_R < 1$.

Injecting E_L in Eq. 17 and 18 and computing the values for the sphere case ($y = R$ and $\dot{y} = \dot{R}$) yields:

$$F_{AM,x} = \rho_L V_b \left[3 C_{AM,x} \frac{\dot{R}}{R} U_{rel} - C_{AM,x} \frac{\partial U_b}{\partial t}\right] \tag{20}$$

with $C_{AM,x} \approx 0.636$.

$$F_{AM,y} = \rho_L V_b \left[-\left(3C_{AM,y1} + C_{AM,y2}\right)\frac{\dot{R}^2}{R} - C_{AM,y1}\ddot{R} + C_{AM,y3}\frac{U_{rel}^2}{R}\right] \tag{21}$$

with $C_{AM,y1} \approx 0.27$, $C_{AM,y2} \approx 0.326$ and $C_{AM,y3} \approx 8.77 \times 10^{-3}$.

Parallel to the wall, the coupled term $\frac{\dot{R}}{R} U_{rel}$ in Eq. 20 promotes detachment and sliding of the bubble if $U_{rel} > 0$ *e.g.* if the bubble is attached to its nucleation site. This agrees with the detaching term of the "two situations" derivations detailed in

2.6.1 and clearly contradicts the aforementioned approach where solely projecting the RPE on both axes lead to an Added-Mass term related to bubble growth that only hinders the departure by sliding. Moreover, we see that accounting for wall presence enhances the added mass coefficient parallel to the wall by approximately 27% compared to Eq. 16 where we have an equivalent $C_{AM,x} = 0.5$. Finally, Eq. 21 exhibits a term induced by the relative velocity that acts as a lift force, which seems to rarely appear in other approaches.

Here we want to insist on the importance on conducting an approach as rigorous as possible when deriving those transient aspects of the force balance. The RPE is only valid for a spherical bubble in an unbounded medium or for a hemispherical bubble laying on a wall as shown by the numerical simulations of Legendre et al. [34]. Otherwise, some terms may be missing and lead to contradictory physical conclusions. Although the proposed method has already been used in different works, we obtained reassessed values of the Added Mass coefficients based on the derivation of the liquid kinetic energy by Van Der Geld. In the spirit of avoiding to introduce extra empirical terms, we keep the Added Mass force as presented in Eq. 20 and 21.

2.7. Force Balance Summary

On Table 1, we sum up some of the mentioned force balances from the literature along with the proposed approach of this paper.

		Klausner (1993) [13]	Thorncroft (2001) [16]	Sugrue (2016) [23]
Forces	$\overline{F_B}$	$\frac{4}{3}\pi R^3 (\rho_L - \rho_V)\,\overline{g}$	$\frac{4}{3}\pi R^3 (\rho_L - \rho_V)\,\overline{g}$	$\frac{4}{3}\pi R^3 (\rho_L - \rho_V)\,\overline{g}$
	$\overline{F_C}$	Eq. 4, $r_w = 0.045$ mm	Eq. 4, $r_w = R\sin(\theta_d)$	Eq. 4, $r_w = 0.025R$
	$\overline{F_{CP}}$	Eq. 5, $R_c = 5R$	Neglected	Eq. 5, $R_c = 5R$
	$\overline{F_D}$	$C_D = \frac{16}{\mathrm{Re}_b}\left[1 + \frac{3}{2}\left(\left(\frac{12}{\mathrm{Re}_b}\right)^n + 0.796^n\right)^{1/n}\right]$, $n = 0.65$	$C_D = \frac{16}{\mathrm{Re}_b}\left[1 + \left(\frac{8}{\mathrm{Re}_b} + \frac{1}{2}\left(1 + \frac{3.315}{\sqrt{\mathrm{Re}_b}}\right)\right)^{-1}\right]$	$C_D = \frac{16}{\mathrm{Re}_b}\left[1 + \frac{3}{2}\left(\left(\frac{12}{\mathrm{Re}_b}\right)^n + 0.796^n\right)^{1/n}\right]$, $n = 0.65$
	$\overline{F_L}$	$C_L = 2.74\sqrt{\mathrm{Sr}} \times \left[\mathrm{Re}_b^{-2} + \left(0.24\sqrt{\mathrm{Sr}}\right)^4\right]^{\frac{1}{4}}$	$C_L = 0.71\sqrt{\mathrm{Sr}} \times \left[\left(\frac{1.15\mathrm{J}(\varepsilon)}{\sqrt{\mathrm{Re}_b}}\right)^2 + \left(\frac{3\sqrt{2\mathrm{Sr}}}{8}\right)^2\right]^{\frac{1}{2}}$	$C_L = 2.74\sqrt{\mathrm{Sr}} \times \left[\mathrm{Re}_b^{-2} + \left(0.24\sqrt{\mathrm{Sr}}\right)^4\right]^{\frac{1}{4}}$
	$\overline{F_{AM}}$	$\frac{3}{2}\rho_L V_b \frac{\dot{R}}{R} U_L \overline{e_x} - \rho_L \pi R^2 \left(\frac{3}{2}\dot{R}^2 + R\ddot{R}\right) \times (\cos(\theta_i)\,\overline{e_y} + \sin(\theta_i)\,\overline{e_x})$, $\theta_i = 10°$	$2\pi\rho_L R^2 \dot{R} U_L \overline{e_x} - \rho_L \pi R^2 \left(\frac{3}{2}\dot{R}^2 + R\ddot{R}\right) \times (\cos(\theta_i)\,\overline{e_y} + \sin(\theta_i)\,\overline{e_x})$, $\theta_i = 45°$	$-\rho_L \pi R^2 \left(\frac{3}{2}\dot{R}^2 + R\ddot{R}\right) \times (\cos(\theta_i)\,\overline{e_y} + \sin(\theta_i)\,\overline{e_x})$, $\theta_i = 10°$

		Mazzocco (2018) [19]	Ren (2020) [20]	Present model
Forces	$\overline{F_B}$	$\frac{4}{3}\pi R^3 (\rho_L - \rho_V)\,\overline{g}$	$\frac{4}{3}\pi R^3 (\rho_L - \rho_V)\,\overline{g}$	$\frac{4}{3}\pi R^3 (\rho_L - \rho_V)\,\overline{g}$
	$\overline{F_C}$	Eq. 4, $r_w = R/15$	Eq. 4, $r_w = 0.2R$	Eq. 4, $r_w = R\sin(\theta)$
	$\overline{F_{CP}}$	Eq. 5, $R_c = 5R$	Eq. 5, $R_c = 5R$	Eq. 5, $R_c = R$
	$\overline{F_D}$	$C_D = 1.13\frac{24}{\mathrm{Re}_b}\left(1 + 0.104\mathrm{Re}_b^{0.753}\right)$	$C_D = \frac{16}{\mathrm{Re}_b}\left[1 + \frac{3}{2}\left(\left(\frac{12}{\mathrm{Re}_b}\right)^n + 0.796^n\right)^{1/n}\right]$, $n = 0.65$	$C_D = C_{D,U}\,(1 + \Delta C_D)$ $C_{D,U}$ by Eq. 8, ΔC_D by Eq. 10
	$\overline{F_L}$	$C_L = 2.61$	$C_L = 2.74\sqrt{\mathrm{Sr}} \times \left[\mathrm{Re}_b^{-2} + \left(0.24\sqrt{\mathrm{Sr}}\right)^4\right]^{\frac{1}{4}}$	C_L by Shi *et al.* [27]
	$\overline{F_{AM}}$	$-\frac{1}{4}\pi\rho_L K^4 (\cos(\theta_i)\,\overline{e_y} + \sin(\theta_i)\,\overline{e_x})$, $\sin(\theta_i) = 0.2$, $\cos(\theta_i) = 1$	$-\rho_L \pi R^2 \left(\frac{3}{2}\dot{R}^2 + R\ddot{R}\right) \times (\cos(\theta_i)\,\overline{e_y} + \sin(\theta_i)\,\overline{e_x})$, $\theta_i = 15°$	$\frac{F_{AM,x}}{\rho_L V_b} = C_{AM,x}\left[3\frac{\dot{R}}{R}U_{rel} - \frac{\partial U_b}{\partial t}\right]$, $C_{AM,x} = 0.636$, $F_{AM,y}$ by Eq. 21.

Table 1: Summary of different force-balance mechanistic approaches.

2.8. Bubble Growth

The question of the bubble growth law during its lifetime including sliding is still an open question that aims to cover various types of heat transfer mechanisms:

- Evaporation due to superheated liquid near the bubble base ;
- Evaporation of a liquid microlayer trapped between the base of the bubble and the wall ;
- Condensation on top of the bubble when it reaches subcooled liquid ;

- Convective heat transfer due to relative velocity between the bubble and the liquid.

To our knowledge, authors that have been tackling this issue had to consider empirical parameters when trying to account for all the above heat transfers. For instance, Zhou [14] and Yoo [35] proposed growth models that consider the previously mentioned mechanisms, introducing many empirical values were used such as:

- The ratio between the bubble projected area and the microlayer area ;
- The fraction of bubble area facing subcooling liquid ;
- Value of coefficients in the condensation law [36].

Moreover, those models postulate the existence of a microlayer contributing to the growth while recent numerical and experimental investigations showed that the bubble may as well grow with a microlayer or in a pure contact line regime depending on the operating conditions [37, 22, 9].

In order to assess the force modeling proposed before, we choose a simpler growth law derived from heat conduction in the superheated liquid layer [38].

$$R\left(t\right) = K\mathrm{Ja}_w\sqrt{\eta_L t} \tag{22}$$

where K is an adjustable constant around the unity depending on the boiling conditions, often expressed as $K = \frac{2b}{\sqrt{\pi}}$. For pool boiling in an uniformly superheated liquid, Plesset & Zwick [38] found $b = \sqrt{3}$, Forster & Zuber [39] obtained $b = \pi/2$ while Zuber [40] stated that values of b should be lying between 1 and $\sqrt{3}$. Similarly, Bhati & Paruya [21] found $1 \leq b \leq \sqrt{5}$. We can thus observe that $K = 2$ is likely to be an upper bound value for the growth constant. This value can logically be lower in the case of subcooled flow boiling. For instance, later comparisons with experimental measurements suggest values of K slightly below 1 for subcooled flow boiling (Figure 8). Yoo *et al.* [35] chose $b = 0.24$ for the diffusive heat flux while accounting for other heat transfer mechanisms.

This type of bubble growth has been widely used, and showed good agreement with many experimental observations and is particularly valid for early growth stages or small bubbles at high pressure [9, 38, 13].

2.9. Liquid Velocity

To compute the liquid velocity and shear rate at bubble center height, we use the wall law of Reichardt [41], which describes the velocity profile from the viscous sublayer to the logarithmic region in a single-phase flow.

$$\begin{aligned} U_L^+ =& \frac{1}{\kappa}\ln\left(1+\kappa y^+\right) + c\left(1 - e^{-y^+/\chi} + \frac{y^+}{\chi}e^{-y^+/3}\right) \\ U_L =& U_L^+ U_\tau \end{aligned} \tag{23}$$

with $\kappa = 0.41$, $\chi = 11$ and $c = 7.8$.

$$\begin{aligned} \frac{\partial U_L^+}{\partial y^+} =& \frac{1}{1+\kappa y^+} + \frac{c}{\chi}\left(e^{-y^+/\chi} + \left(1 - \frac{y^+}{3}\right)e^{-y^+/3}\right) \\ \frac{\partial U_L}{\partial y} =& \gamma = \frac{U_\tau^2}{\nu_L}\frac{\partial U_L^+}{\partial y^+} \end{aligned} \tag{24}$$

The friction velocity is computed using Mac Adams correlation [42].

$$U_\tau = \sqrt{\frac{\tau_w}{\nu_L}} \tag{25}$$

$$\tau_w = 0.018\ \mathrm{Re}_{D_h}^{-0.182}\ \rho_L \left\langle U_L \right\rangle^2 \tag{26}$$

3. Departure by Sliding

3.1. Non-Dimensional Analysis

Now that the force balance has been established, we can write it parallel to the wall before bubble departure by sliding, considering that the bubble is immobile *i.e.* $U_b \ll U_L$ and $\frac{\partial U_b}{\partial t} \approx 0$.

$$\begin{aligned} -\pi R\sigma f_{C,x} + \frac{4}{3}\pi R^3\left(\rho_L - \rho_V\right)g + \frac{1}{2}C_D\rho_L\pi R^2 U_L^2 \\ + \frac{4}{3}\pi R^3\rho_L\ 3C_{AM,x}\frac{\dot{R}}{R}U_L = 0 \end{aligned} \tag{27}$$

$$f_{C,x} = 2.5\ \frac{\mathrm{d}\theta}{(\pi/2)^2 - \mathrm{d}\theta^2}\sin\left(\theta\right)\cos\left(\mathrm{d}\theta\right)$$

with $f_{C,x} \to 0$ if $\mathrm{d}\theta \to 0$.

We can note that the departure by sliding is promoted by the Buoyancy, the Drag and the Added Mass forces. Only the Capillary force keeps the bubble attached to its nucleation site, which will be discussed later.

Re-writing Eq. 27 in non-dimensional form by dividing the LHS by the Added Mass force yields:

$$-\frac{1}{2}\frac{f_{C,x}}{K^2 C_{AM,x}}\frac{1}{\mathrm{Ca}}\frac{\mathrm{Pr}_L}{\mathrm{Ja}_w^2}+\frac{1}{3}\frac{1}{K^2 C_{AM,x}}\frac{\mathrm{Re}_b}{\mathrm{Fr}}\frac{\mathrm{Pr}_L}{\mathrm{Ja}_w^2}+\frac{1}{8}\frac{C_D}{K^2 C_{AM,x}}\mathrm{Re}_b\frac{\mathrm{Pr}_L}{\mathrm{Ja}_w^2}+1=0 \tag{28}$$

where we have the following non-dimensional numbers:

$$\mathrm{Re}_b=\frac{2RU_L}{\nu_L}\ ;\ \mathrm{Fr}=\frac{\rho_L U_L^2}{(\rho_L-\rho_V)\,gR}\ ;\ \mathrm{We}=\frac{\rho_L U_L^2 R}{\sigma}\ ;\ \mathrm{Eo}=\frac{(\rho_L-\rho_V)\,gR^2}{\sigma}\ ;$$
$$\mathrm{Ja}_w=\frac{(T_w-T_{sat})\,\rho_L c_{P,L}}{\rho_V h_{LV}}\ ;\ \mathrm{Pr}_L=\frac{\nu_L}{\eta_L}\ ;\ \frac{\dot{R}}{U_L}=\frac{K^2\mathrm{Ja}_w^2}{\mathrm{Pr}_L\mathrm{Re}_b}\ ;\ \mathrm{Ca}=\frac{\mu_L U_L}{\sigma}$$

Eq. 28 exhibits terms that can be used to compare the magnitude of each detaching forces. We can obtain the following conditions:

$$\text{Added Mass greater than Drag if: } \frac{\mathrm{Ja}_w^2}{\mathrm{Pr}_L}>\frac{1}{8}\frac{C_D}{C_{AM,x}}\frac{1}{K^2}\mathrm{Re}_b \tag{29}$$

$$\text{Added Mass greater than Buoyancy if: } \frac{\mathrm{Ja}_w^2}{\mathrm{Pr}_L}>\frac{1}{3}\frac{1}{C_{AM,x}K^2}\frac{\mathrm{Re}_b}{\mathrm{Fr}} \tag{30}$$

$$\text{Drag greater than Buoyancy if: } \mathrm{Re}_b>\frac{16}{3}\frac{1}{C_D}\frac{\mathrm{Eo}}{\mathrm{Ca}}=\mathrm{Re}_c \tag{31}$$

Those boundaries can be plotted on a $\left(\mathrm{Ja}_w^2/\mathrm{Pr}\ ;\ \mathrm{Re}_b\right)$ map for a given fluid and bubble diameter $D=2R$, an example of such a map is presented on Figure 3a. This allows to visualize the operating conditions under which each of the detaching forces will be dominant. Logically, Buoyancy dominates for low Re_b regimes contrary to Drag. Added Mass dominates when values of $\mathrm{Ja}_w^2/\mathrm{Pr}_L$ are high *i.e.* when bubble grows rapidly.

3.1.1. Influence of Pressure

On Figure 3b, we draw the dominance map for 3 different pressures and associated orders of magnitude of bubble departure diameter [43].

The impact of pressure is mostly seen through the decrease of bubble departure diameter. As pressure increases, Buoyancy force decreases while Drag and Added Mass forces display much larger dominance zones. The competition between those two terms mainly relies on the competition between liquid flow velocity and wall superheat or heat flux.

3.1.2. Comparison between Fluids

On Figure 3c, we compare the dominance zones for R12 at 26 bar and water at 155 bar. Moderately pressurized R12 (10 to 30 bar) has often been used as a simulating fluid to mimic water in PWR since it has the same density ratio and Weber number for instance.

Assuming that the conservation of Weber and Boiling numbers may lead to similar bubble departure diameters, we can observe that the boundaries between the two fluids are very close. This qualitatively indicates that R12 shall present bubble departure by sliding mechanisms similar to what happens in PWR, which could comfort the confidence one may have in extrapolating the observations done using the simulating fluid to industrial applications.

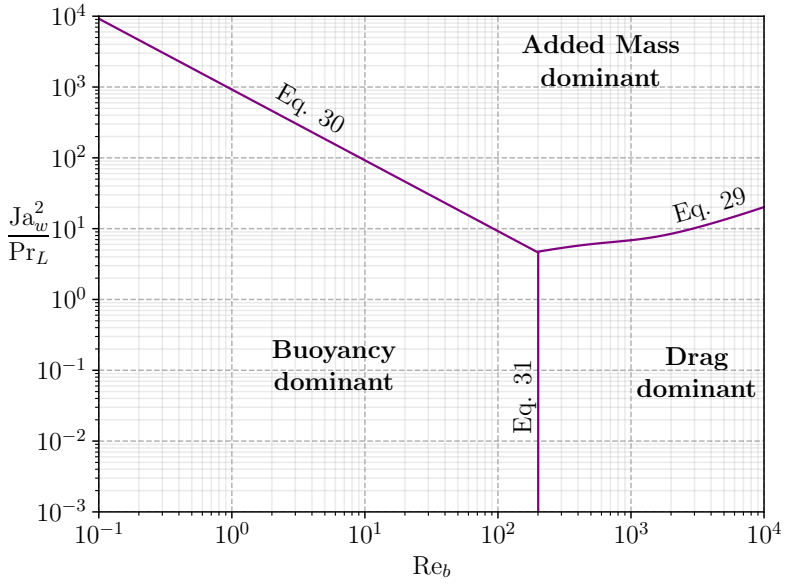

(a) Dominance map regarding departure by sliding. Boundaries plotted for water at 1 bar and $D_d = 0.5$mm.

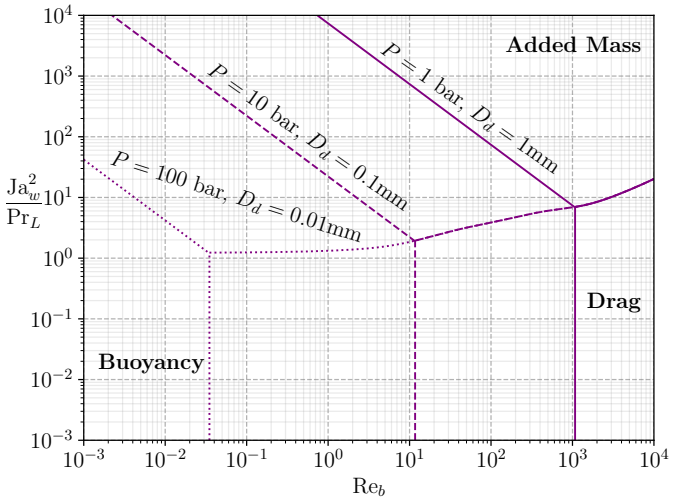

(b) Dominance map plotted for water at different pressures and bubble departure diameters.

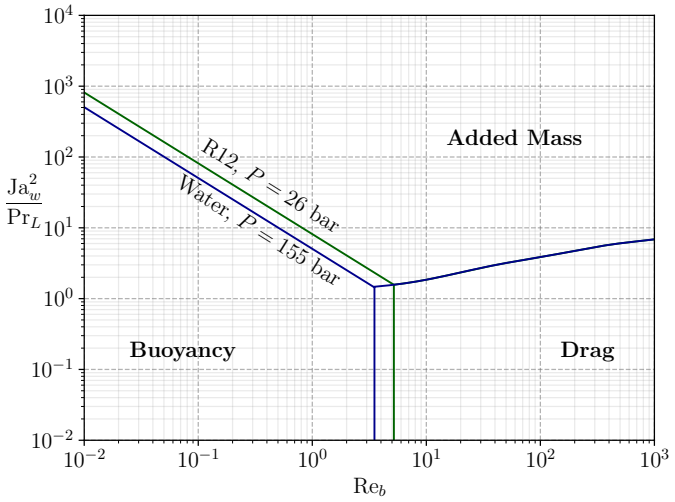

(c) Dominance map for R12 as simulating fluid for PWR. $D_d = 0.05$mm chosen according to R12 measurements [50] with bubbles of ~ 0.1mm diameter after lift-off. The same value is taken for water.

Figure 3: Examples of qualitative analysis using the non-dimensional regime map.

3.2. Application to Experimental Data

Now we want to apply this non-dimensional approach to experimental measurement in order to determine the actual bubble departure by sliding regimes. We rely on 7 experiments in which bubble departure diameters in vertical flow boiling were measured. The operating conditions are gathered in Table 2.

If the value of ΔT_w is not available in the considered data-set, we estimate ΔT_w using Frost & Dzakowic correlation [44].

$$\Delta T_w = \mathrm{Pr}_{L,sat}\sqrt{\frac{8\sigma\phi_w T_{sat}}{\lambda_L \rho_V h_{LV}}} \tag{32}$$

Author	Fluid	D_h [mm]	P [bar]	G_L [kg/m^2/s]	ΔT_L [K]	ϕ_w [kW/m^2]	ΔT_w [K]	D_d [mm] (N_{mes})
Thorncroft [48] (1998)	FC-87	12.7	N.A.	0 - 319	0.99 - 3.27	2.83 - 11.8	0.54 - 6.89	0.094 - 0.237 (10)
Maity [7] (2000)	Water	20	1.01	0 - 239.6	0.3 - 0.7	N.A.	5 - 5.9	0.788 - 1.71 (9)
Chen [51] (2012)	Water	3.8	1.2 - 3.35	214 - 702	14.5 - 30.3	83.6 - 334	N.A.	0.549 - 2.255 (22)
Sugrue [23] (2014)	Water	16.6	1.01	250 - 400	10 - 20	50 - 100	2 - 6	0.229 - 0.391 (16)
Guan [30] (2014)	Water	9	1.01	87.3 - 319.2	8.5 - 10.5	68.2 - 104	4.5 - 8.5	0.62 - 1.85 (12)
Ren [20] (2020)	Water	3.8	2 - 5.5	488.4 - 1654	28.7 - 51	160.7 - 643.2	N.A.	0.045 - 0.111 (42)
Kossolapov [9] (2021)	Water	11.8	19.9 - 39.8	500 - 1500	10	178 - 613	10.0 - 16.2*	0.01 - 0.047 (11)

Table 2: Bubble departure diameters data sets in vertical flow boiling.
*ΔT_w values were recalculated based on fitted growth profiles proposed by Kossolapov [9].

To place experimental measurements on the non-dimensional map, we need a bubble detachment diameter value D_d to plot the dominance zones. Since measured D_d vary significantly in each experiment, we draw the boundaries for the maximum and minimum values of D_d as shown on Figure 4a. The range of bubble diameter is given in Table 2. If the considered data covers different pressures, boundaries for each pressure are plotted to exhibit its impact (Figures 4d, 4e and 4f). We chose a value of $K = 1$ to draw the boundaries.

The Figure 4 shows that for most of the low pressure experiments, the detaching forces are the Added Mass and the Buoyancy forces. Smaller bubbles are mainly detached under the effect of the Added Mass force (Figures 4c, 4d and 4e). When the bubbles detach at higher diameters, the impact of the Buoyancy force naturally increases and is comparable to the Added Mass force (Figures 4a and 4b).

When the pressure increases, we observe that the experimental measurements gradually move towards the Drag dominant zone as seen on Figures 4e and 4f. This main difference in the dynamic regime when bubble departs by sliding arises from multiple effects:

- The decrease of ρ_L/ρ_V with pressure, thus reducing Ja_w and the impact of the detaching Added Mass term ;
- The higher liquid mass fluxes in Kossolapov experiments, increasing the impact of the Drag ;
- The decrease of D_d with pressure, reducing the magnitude of Buoyancy.

However, we see that some measurements lie close to the Added Mass / Drag boundary (Figure 4f), indicating that the Added Mass force still plays a significant role for bubble detachment. This means that regardless of the operating pressure, the detaching term associated to the coupling between bubble growth and outer liquid flow should not be neglected in the force balance (Eq. 20).

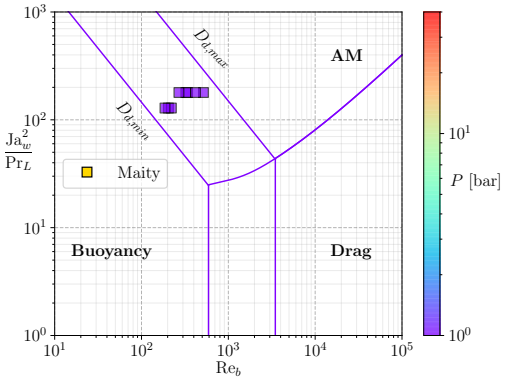

(a) Maity data

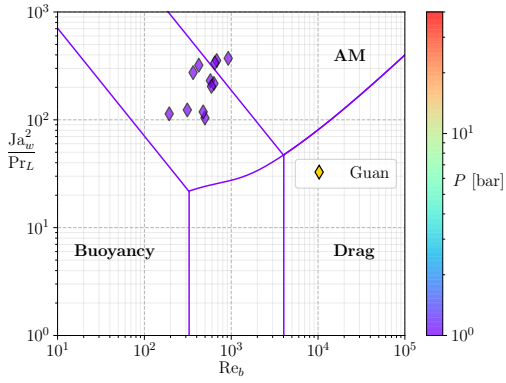

(b) Guan data

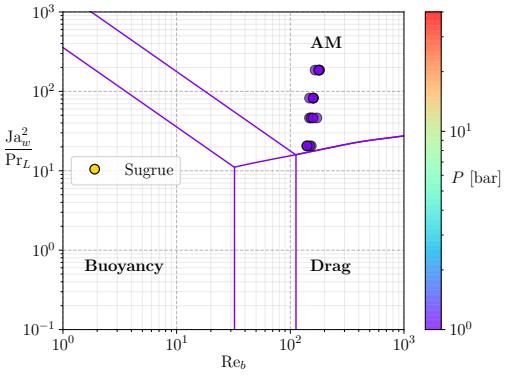

(c) Sugrue data

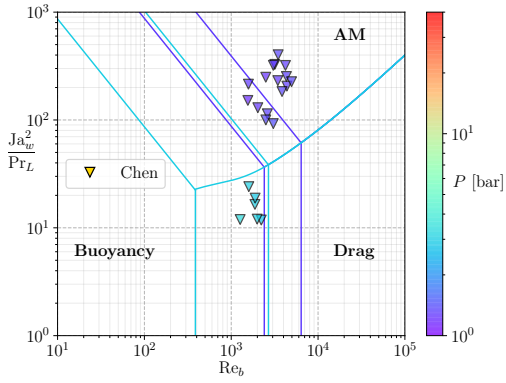

(d) Chen data

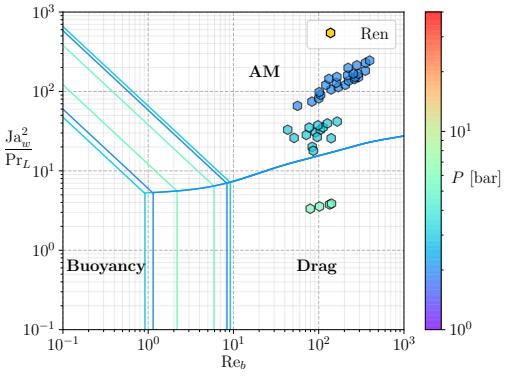

(e) Ren data

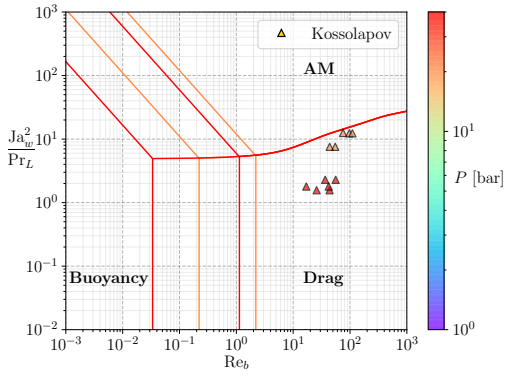

(f) Kossolapov data

Figure 4: Dominance maps for each water data sets from Table 2.

3.3. Departure Diameter Prediction

3.3.1. About the Use of Empiricism

As previously mentioned, the case of bubble detachment in vertical flow boiling is particular since only one force maintains the bubble attached to its nucleation site: the Capillary force (Eq. 4). Its expression depends on the contact angle θ, the angle half-hysteresis dθ and the bubble foot radius r_w (or ratio to bubble diameter r_w/R) and is thus very sensitive to those values. Paradoxically, those terms are among the least precisely known due to the difficulty of measurement and associated uncertainties. For instance, conducting precise evaluations of the contact angle near the bubble base through optical techniques can be challenging because of the strong temperature gradients close to the heated surface.

Consequently, empirical choices have to be made in order to set a value to those parameters, often by relying on data-fitting or approximate measurements in other conditions. For instance, contact angles are often taken as arbitrary average values [20] or measurements in room conditions [23] and applied over a whole set of experiments. This is questionable since contact angle is unlikely to remain unchanged over different operating conditions and surfaces with varying roughness and properties [45].

However, no better information except those given by the authors can be used to evaluate the Capillary force since no generic model exists to compute the contact angle and hysteresis. In this work, admitting a significant uncertainty (typically 5°, as in Guan *et al.* [30]), we will use the following values for the contact angles :

- $\theta_u = 25.3°$ and $\theta_d = 6.6°$ for Thorncroft data (measured values for FC-87 on nichrome [16]) ;
- $\theta_u = 50°$ and $\theta_d = 40°$ for Maity data (measured average contact angles for each bubble during its lifetime [7]) ;
- $\theta_u = 130°$ and $\theta_d = 65°$ for Chen data (chosen values in their study following measurements for water on stainless steel at high temperature by Kandlikar *et al.* [46]) ;
- $\theta_u = 91°$ and $\theta_d = 8°$ for Sugrue data (measured values at room temperature [18]) ;
- $\theta_u = 75°$ and $\theta_d = 30°$ for Guan data (measured average value through experimental visualizations [30]) ;
- $\theta_u = 45°$ and $\theta_d = 36°$ for Ren data (chosen values in their study [20]) ;

- $\theta = 80°$ for Kossolapov data (typical contact angle for water on ITO [9]) and $\mathrm{d}\theta = 0.5°$ assuming that the very small bubbles at high pressure are nearly not tilted.

Similarly, the bubble foot radius r_w is often empirically assumed to be either constant [13] proportional to the bubble radius [23, 19] or to follow a linear or logarithmic law of R [14, 30]. That is why we chose to use the truncated sphere hypothesis (Eq. 2) to compute r_w using R and θ.

Finally, we would like to acknowledge that the empiricism to evaluate those parameters represents one of the biggest flaws of the force-balance approach. Indeed, such a model aims to detect small sign changes in a sum of a few μN of forces that are decades larger as pointed out by Bucci *et al.* [47]. Mechanistic models are thus strongly sensitive to any extra parameter included in the modeling of the forces.

3.3.2. Growth Constant Value

Since the value $K \approx 2$ represents an upper bound for the growth constant in a quiescent uniformly superheated liquid (Subsection 2.8) and that values below 1 can be a better fit for bubble growth in subcooled flow boiling (Figure 8), we choose the value proposed by Yoo *et al.* growth model [35] for the diffusive heat flux from the superheated liquid layer, validated with different working fluids in subcooled boiling:

$$K = \frac{2b}{\sqrt{\pi}}, \; b = 0.24 \tag{33}$$

3.3.3. Predictions

We consider the non-dimensional force balance before departure.

$$C_{AM,x} K^2 \frac{\mathrm{Ja}_w^2}{\mathrm{Pr}_L} + \frac{1}{3}\frac{\mathrm{Re}_b}{\mathrm{Fr}} + \frac{1}{8} C_D \mathrm{Re}_b = \frac{1}{2}\frac{f_{C,x}}{\mathrm{Ca}} \tag{34}$$

Since we only have the capillary term hindering departure as a first approach, we can suppose that departure is reached when:

$$C_{AM,x} K^2 \frac{\mathrm{Ja}_w^2}{\mathrm{Pr}_L} + \frac{1}{3}\frac{\mathrm{Re}_b}{\mathrm{Fr}} + \frac{1}{8} C_D \mathrm{Re}_b > \frac{1}{2}\frac{f_{C,x}}{\mathrm{Ca}} \tag{35}$$

which is similar to considering that the other forces overcome the Capillary force.

On Figure 5, we show the predictions obtained with the proposed modeling and those obtained with Mazzocco's recent model [19].

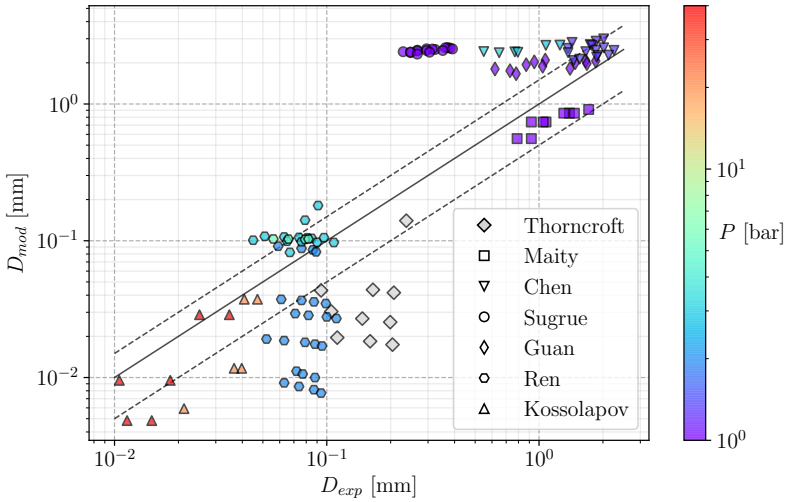

(a) Proposed model without accounting for contact angle uncertainties

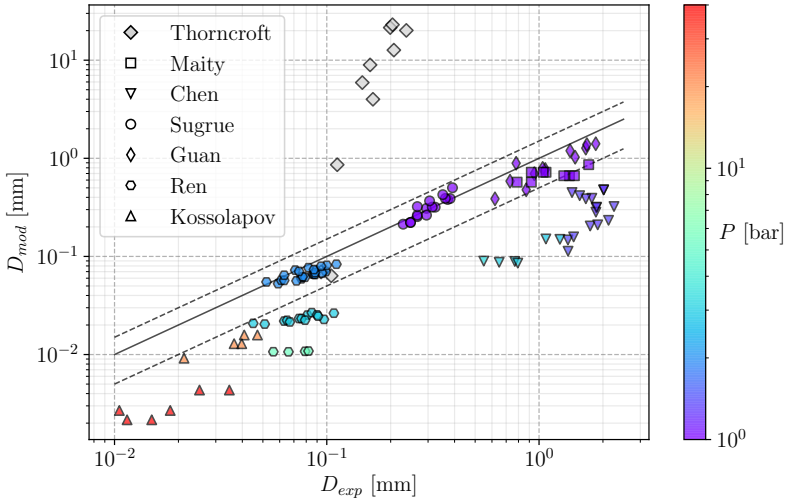

(b) Mazzocco model

Figure 5: Predicted bubble departure diameters

The model have an acceptable trend on some experimental sets, but strong overestimations occur on the cases of Sugrue. Moreover, we observe significant underestimations on the data of Ren at 2 bar and Thorncroft.

Mazzocco's model provides a good accuracy on the data of Sugrue, Guan, Maity and Ren (2 bar). However, we observe very large overestimation over Thorncroft's

measurements and significant underestimation on Chen, Ren (3 and 5 bar) and Kossolapov measurements.

3.4. Discussion and accounting for parameters uncertainties

The aforementioned errors observed for the proposed model may originate from various reasons:

- The contact angle proposed for Sugrue cases is high with a large hysteresis, suggesting strongly deformed and flattened bubbles under the truncated sphere hypothesis. Based on images from Sugrue's work [18], a comparison between a real bubble with the assumed shape is presented on Figure 6. This shows a huge difference which indicates that the contact angle and hysteresis values may be overestimated. Using the available images, the ratio of the bubble diameter to the apparent bubble foot would lead to an average contact angle $\theta \approx 20°$ for a truncated sphere. Noting that a larger inclination is observed for the bubbles under higher mass fluxes leads us to suppose a value $\mathrm{d}\theta \approx 15°$. This represent a similar inclination to contact angle ratio ($\mathrm{d}\theta/\theta$) compared to the initially proposed values. The resulting new shape is also presented on Figure 6 and seems to better represent the actual bubble.

- For cases where limited under and overestimation is observed, we may allow to account for an uncertainty as high as 5° for the average contact angle θ and half-hysteresis $\mathrm{d}\theta$.

- As mentioned earlier, applying the same contact angle and hysteresis over a wide range of measurements is a strong assumption, especially for cases where different pressures and bubble diameter variations are observed. Thus, we may slightly distinguish the applied values of θ and $\mathrm{d}\theta$ for different pressures within a given experiment, keeping a change no larger than 5°.

- Kossolapov cases at $G_L = 500$ kg/m^2/s are better predicted. Cases under higher mass fluxes (1000 and 1500 kg/m^2/s) present underestimation that could come from the value of $\mathrm{d}\theta$. At such mass fluxes, the Weber number can be up to a decade higher and bubbles may thus accept a larger inclination before detachment.

- Cases of Ren and Chen rely on chosen values for θ and $\mathrm{d}\theta$ and not on measured ones. They are therefore subject to strong uncertainties. We can note that the values for Chen cases are significantly high.

- The proposed growth law is still rather simple and may miss significant information, especially regarding bubble size and fluid properties such as the Prandtl number.

- Errors on Thorncroft cases may be linked to uncertainties regarding FC-87 properties. Indeed, we use the values given at $T_{sat} = 29°$ at 1 bar in his work [48]. However, the saturation temperature indicated in his test matrix is close to 40° which means that measurements were conducted at a higher pressure, for which we do not have FC-87 properties.

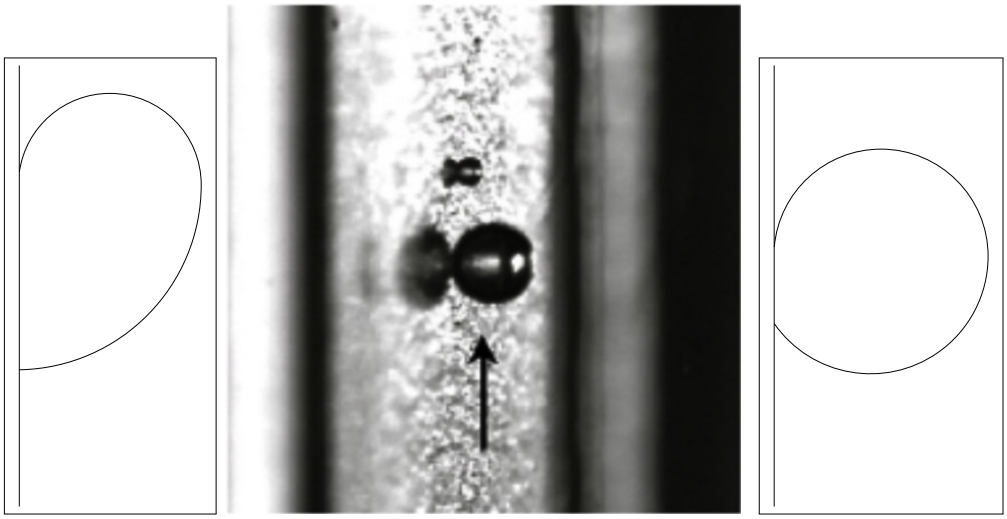

Figure 6: Initially assumed, real and reassessed bubble shape for Sugrue cases (picture adapted from [18]).

Therefore, using modified values of θ and dθ among experimental data sets with no more than a 5° change (except for Sugrue cases reassessed values) leads to predictions on Figure 7.

The predictive capacity of the model is significantly enhanced, especially on Sugrue's cases which tends to indicate that the contact angle reassessment was justified under the truncated sphere hypothesis. Table 7c summarizes the average errors obtained with the present model and Mazzoco's one.

The proposed model achieves an overall better predictive capability even when excluding measurements from Thorncroft on which Mazzocco's model strongly overestimates the departure diameter. Mazzocco's model is still better on Sugrue and Guan cases since it was built and validated using those measurements. It better

Author	θ [°]	dθ [°]
Thorncroft	21	14
Maity	45	10
Chen	92.5	27.5
Sugrue	20	15
Guan	47.5	17.5
Ren (2 bar)	45.5	7.5
Ren (3 bar)	37.5	3.5
Ren (5 bar)	35.5	3.5
Koss. (500 kg/m^2/s)	80	0.5
Koss. (1000 kg/m^2/s)	80	1
Koss. (1500 kg/m^2/s)	80	1.5

(a) Modified contact angle and hysteresis values.

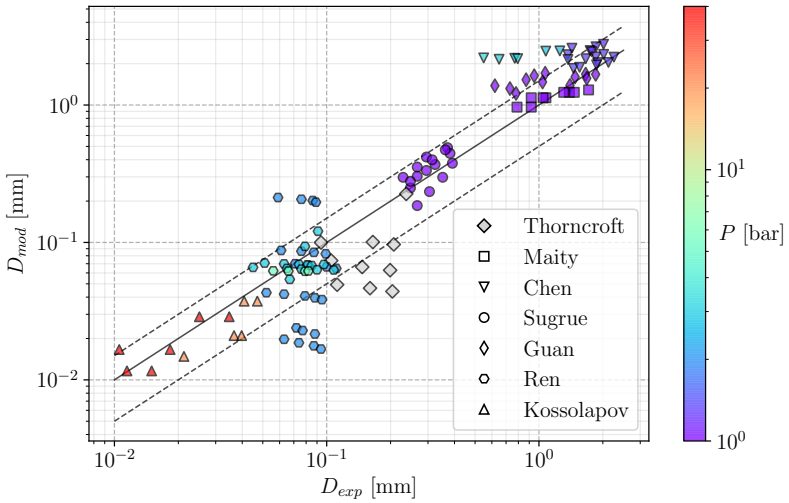

(b) Predicted bubble departure diameters.

Author	Mazzocco	Present model
Thorncroft	4874%	46.2%
Maity	39.7%	13.3%
Chen	83.8%	73.6%
Sugrue	9.73%	21%
Guan	25.5%	44.5%
Ren	40.32%	47%
Kossolapov	73.95%	24.2%
Total (without Thorncroft)	46.16%	43.3%

(c) Proposed model performance while accounting for contact angle uncertainties and error comparisons with Mazzocco *et al.* model.

Figure 7: Errors achieved by the model and Mazzoco *et al.* model.

predicts results from Ren but only for the 2 bar cases while it underestimates the departure diameter for higher pressures. Those results are a coupled effect of his optimized growth law along with the imposed value of r_w/R and the use of the inclination angle to hinder departure as mentioned in 2.6.

The approach demonstrated the importance and the strong influence of the contact angle and hysteresis. A small change of their value (staying in the uncertainty range of 5°) allowed to reach reasonable predictions over a large range of bubble departure diameters with the model of this paper, using a reduced number of empirical parameters.

4. Sliding phase

4.1. Modeling

After departure, bubbles slide over a distance l_{sl} which scales the impact of the sliding phenomenon over the wall heat transfer. Achieving good prediction of bubble sliding velocity is then important if one wishes to correctly quantify its impact.

Following the force balance framework presented in Section 2, we can write Newton's second law parallel to the wall for the sliding bubble.

$$\begin{aligned}\rho_V \frac{\mathrm{d}(V_b U_b)}{\mathrm{d}t} =& -\pi R\sigma f_{C,x} + \frac{4}{3}\pi R^3 \left(\rho_L - \rho_V\right) g + \frac{1}{2} C_D \rho_L \pi R^2 U_L^2 \\ &+ \frac{4}{3}\pi R^3 \rho_L \left[3 C_{AM,x} \frac{\dot{R}}{R} U_{rel} - C_{AM,x} \frac{\mathrm{d}U_b}{\mathrm{d}t}\right]\end{aligned} \tag{36}$$

This equation can be re-written to express the bubble acceleration.

$$\begin{aligned}\left(1 + \frac{\rho_L}{\rho_V} C_{AM,x}\right) \frac{\mathrm{d}U_b}{\mathrm{d}t} =& \left(\frac{\rho_L}{\rho_V} - 1\right) g + \frac{3}{8} \frac{C_D}{R} \frac{\rho_L}{\rho_V} \left(U_L - U_b\right) \left|U_L - U_b\right| \\ &+ 3\frac{\dot{R}}{R}\left[C_{AM,x} \frac{\rho_L}{\rho_V} \left(U_L - U_b\right) - U_b\right] - \frac{3}{4} \frac{\sigma}{\rho_V} \frac{f_{C,x}}{R^2}\end{aligned} \tag{37}$$

Then, we numerically solve this equation from the moment when $R \geq R_d$ using a first order Euler scheme for a duration close to the experimental sliding time. To assess the accuracy of Eq. 37 and achieve separate-effect validation, we modify the growth constant K in order to roughly match experimental radius measurements. The goal is to verify if the force balance allows a good prediction of bubble velocity provided a correct bubble growth. Next sections compare obtained results against low and high pressure data.

4.2. Low Pressure Sliding

Maity [7] provided simultaneous measurements of bubble radius and velocity over time in vertical boiling for three liquid mass fluxes near saturation conditions. The contact angles were kept the same as in 3.3 since Maity provided average values over the bubble lifetime.

Results are displayed on Figure 8. The model seems to fairly good predict bubble sliding velocity for the 3 cases. The moment of departure is a bit underestimated as previously observed (Figure 5).

The biggest discrepancy is observed for the case at $G_L = 143.8$ kg/m^2/s. The slope of the velocity profile is close to the experiments, but the bubble reaches a nearly constant acceleration too rapidly which yields an approximately constant overestimation of 0.1 m/s.

The case at $G_L = 239.6$ kg/m^2/s is well predicted regarding the velocity. However, the growth profile was difficult to match since measurements exhibit significant changes in growth regime after departure, which is probably due to the bubble being large enough to be impacted by the bulk flow and recondensation. A finer model for bubble growth could be of interest here.

We can note that values of K between 0.5 and 1 were used to better fit the bubble radius time profile.

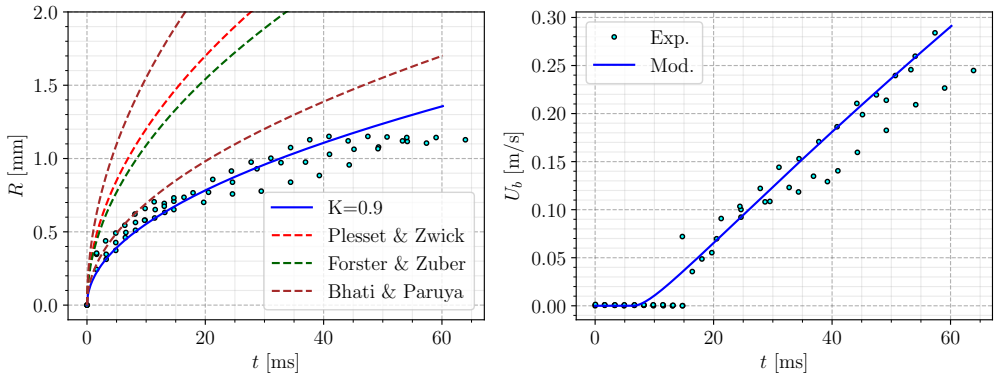

(a) $\Delta T_w = 5.0°\text{C}$, $G_L = 73.8$ kg/m^2/s

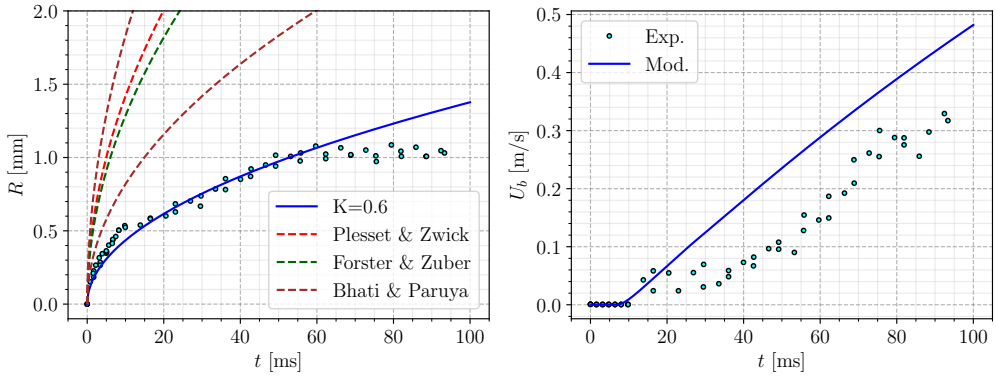

(b) $\Delta T_w = 5.9°\text{C}$, $G_L = 143.8$ kg/m^2/s

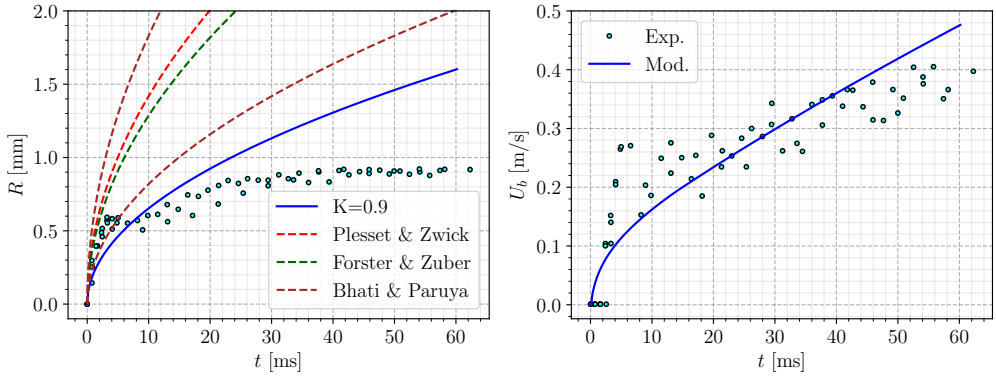

(c) $\Delta T_w = 5.9°\text{C}$, $G_L = 239.6$ kg/m^2/s

Figure 8: Bubble sliding velocity predictions on Maity cases - Plesset & Zwick : $K = \frac{2\sqrt{3}}{\sqrt{\pi}}$ - Forster & Zuber : $K = \sqrt{\pi}$ - Bhati & Paruya : $\frac{2}{\sqrt{\pi}} \leq K \leq \frac{2\sqrt{5}}{\sqrt{\pi}}$

4.3. High Pressure Sliding

In his work, Kossolapov [9] conducted measurements of radius and sliding length over thousands of individual bubbles and then provided the associated statistical distributions. To compare our model with his measurements, we took the upper and lower bounds of R and l_{sl} over time and plotted the associated bands of measured values as shown on Figure 9.

Comparisons were done for cases at 20 bar and 40 bar and 3 different values of G_L. The value of $\mathrm{d}\theta$ for the simulations was kept really small (2° at 20 bar and 0.5° at 40 bar) since bubble tilt is supposed to reduce during sliding because the relative velocity regarding the liquid flow is diminishing. Moreover, higher pressure means smaller bubbles that are even more unlikely to present a significant contact angle hysteresis. We also want to mention that neglecting the capillary term in Eq. 37 had a minor impact over the results except that the bubble accelerates a little bit faster.

The obtained results are in good agreement with the sliding length profile vs. time, which means bubble sliding velocity is well predicted for those cases.

Once the estimation of ΔT_w using Eq. 32 is corrected as mentioned in 3.2, values of K between 0.8 and 1.3 reasonably fits the bubble radius measurements.

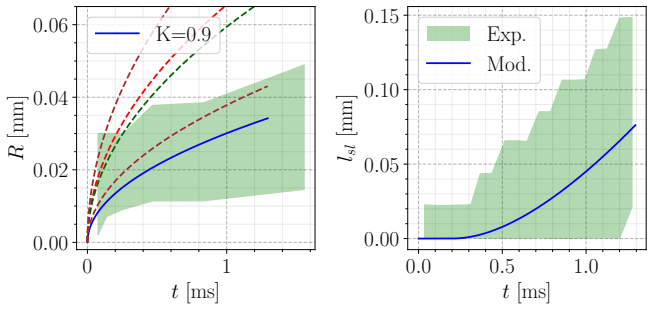

(a) $P = 20$ bar, $G_L = 500$ kg/m^2/s, $\Delta T_w = 12.6$K

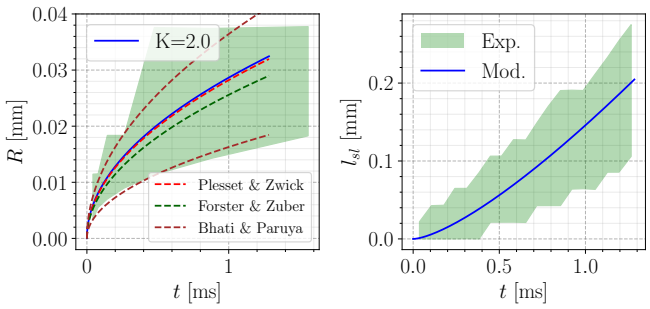

(b) $P = 40$ bar, $G_L = 500$ kg/m^2/s, $\Delta T_w = 10.1$K

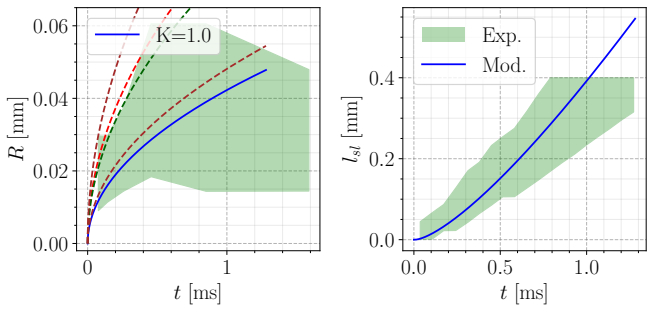

(c) $P = 20$ bar, $G_L = 994$ kg/m^2/s, $\Delta T_w = 16.1$K

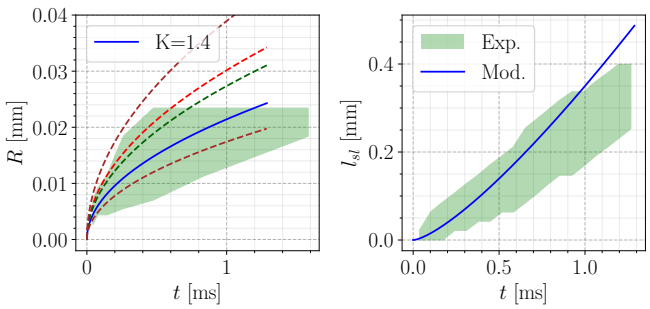

(d) $P = 40$ bar, $G_L = 994$ kg/m^2/s, $\Delta T_w = 10.8$K

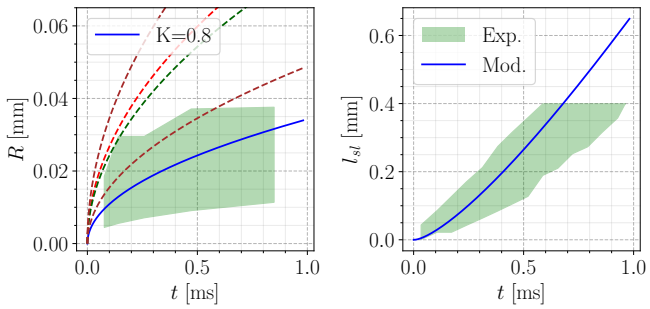

(e) $P = 20$ bar, $G_L = 1504$ kg/m^2/s, $\Delta T_w = 16.2$K

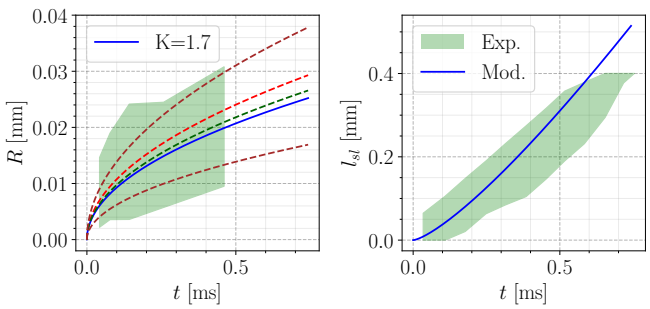

(f) $P = 40$ bar, $G_L = 1504$ kg/m^2/s, $\Delta T_w = 12.2$K

Figure 9: Bubble sliding length predictions on Kossolapov cases - Plesset & Zwick : $K = \frac{2\sqrt{3}}{\sqrt{\pi}}$ - Forster & Zuber : $K = \sqrt{\pi}$ - Bhati & Paruya : $\frac{2}{\sqrt{\pi}} \leq K \leq \frac{2\sqrt{5}}{\sqrt{\pi}}$

4.4. Comparison of Forces in Sliding Stage

In order to identify the main accelerating forces, we compare the amplitude of the forces during the sliding phase for one low pressure case of Maity and one high pressure case of Kossolapov (Figure 10). It appears that at high pressure and liquid velocity, the Drag force is the main driving force and stays positive since the bubble do not slide faster than the rapid surrounding liquid (reaching approximately 80% of the local liquid velocity). On the other hand, larger bubbles observed at low pressure and liquid velocity are accelerated by Buoyancy due to their larger volume, with a nearly negligible Drag force. In both cases, the Added Mass force can not be neglected especially when bubble velocity rises by limiting its acceleration induced by the larger force (Buoyancy or Drag in the presented cases). This further emphasizes the importance of a proper derivation of the Added Mass force regardless of the boiling conditions. The Capillary force seems to be a limited but constant slowing term in both cases. Finally, the amplitude of the forces involved can span from roughly 10×10^{-4} N at low pressure (much greater than the rate of change of bubble momentum laying around 10^{-9} N) down to a few nN at higher pressure (same order of magnitude as the rate of change of bubble momentum), especially due to the bubble size.

This comparison highlights the fact that the proposed model is able to represent different forces hierarchy depending on the flow conditions and to acceptably predict the associated bubble sliding velocity, which is an encouraging point regarding its generality.

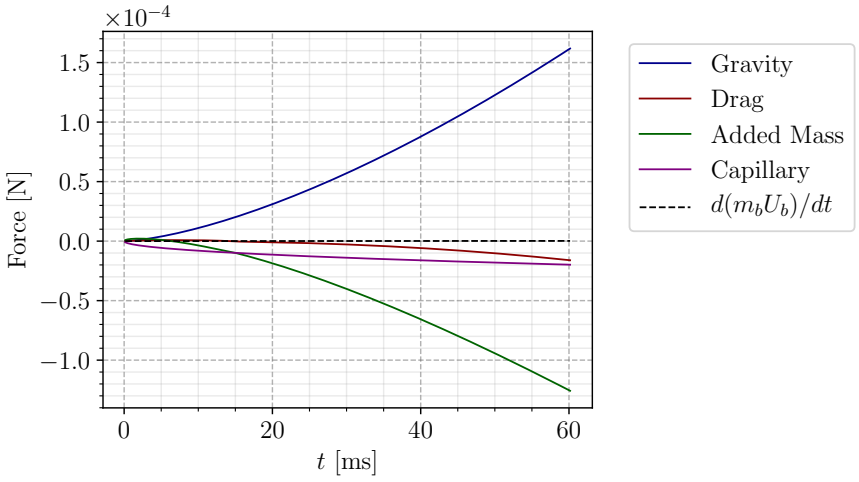

(a) Maity : $\Delta T_w = 5.9°$ C, $G_L = 239.6$ kg/m^2/s

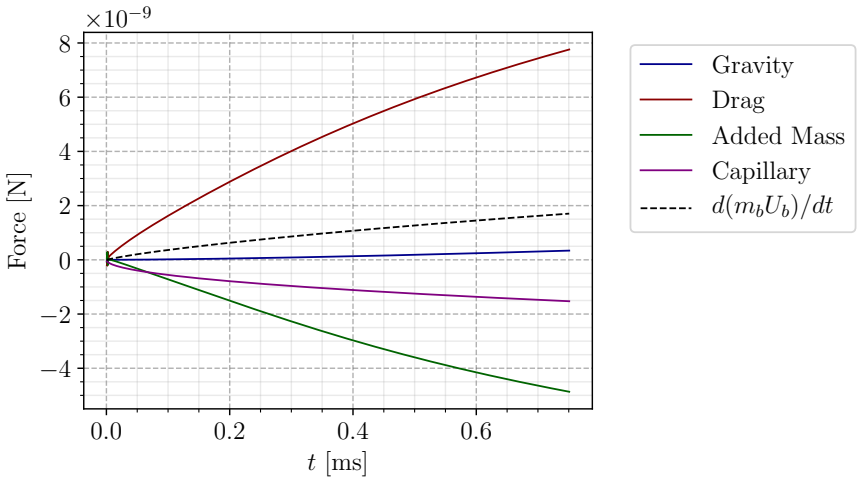

(b) Kossolapov : $\phi_w = 0.613$ MW/m^2, $G_L = 1504$ kg/m^2/s

Figure 10: Amplitude of each force during sliding

5. Conclusion

In this work, we proposed a new expression of the force balance for a single bubble in a vertical upward boiling flow, including updated expressions for the drag and added mass forces. This force balance was then used to study bubble departure by sliding and compared with bubble departure diameter and sliding velocity measurements. The main highlights of this study are:

- A global force balance that avoids including extra empirical parameters. We notably get rid of empirical choices regarding bubble foot radius and bubble radius of curvature at its foot.
- The use of a recent formulation to compute the Drag coefficient thanks to DNS results of Shi *et al.* [27].
- Reassessed computation of the Added Mass force and associated coefficients from the expression of the liquid kinetic energy proposed by Van Der Geld [33], which lead to a unified calculation for a truncated spherical bubble growing on a wall in a flow.
- A non dimensional approach leading to force regime maps to qualitatively determine the dynamic regime in which bubbles are departing from the nucleation site. It shows that the detaching Added Mass term due to external liquid flow is rarely negligible and often dominates at low pressure. Increasing pressure mostly leads to Drag dominant regimes.
- Bubble departure diameter predictions are achieved with a reasonable accuracy over a large range of measured values from 7 data sets. This could be reached by accepting an uncertainty of 5° for the values of the contact angle θ and half-hysteresis $\mathrm{d}\theta$ to which the model was sensitive. This indicates that using fixed values for large data sets seems incorrect and that extra empiricism may not be needed if a proper modeling of those parameters was achieved. For the estimation of the Added Mass force, the model of Yoo *et al.* [35] for the diffusive heat flux from the superheated liquid has been chosen to estimate the bubble growth rate.
- Bubble sliding velocity simulations showed a good agreement with experimental observations at low pressure provided a correct bubble growth profile. The agreement is also reasonable at high pressure.

- Comparison of forces at stake showed that Buoyancy and Drag forces are respectively mainly responsible for bubble acceleration at low and high pressure. As for the departure, Added Mass is not negligible regardless of the flow conditions.

- The final formulation of the model requires the knowledge of three parameters: the bubble growth rate K, the static contact angle θ and the contact angle hysteresis $\mathrm{d}\theta$. To remain physically consistent, those should not be chosen at random but rather rely on values following experimental or theoretical approaches corresponding the aimed physical conditions.

The limitations of the developed approach lie mainly in its sensitivity to the value taken for the growth constant K (Eq. 33). To avoid a fitting of the experimental values, the modeling of the bubble growth could be enriched by a clean modeling of the bubble growth including effects such as condensation, microlayer evaporation and impact of the external liquid flow. Existing models rely on empirical values which thus reduces their general applicability outside of their validation range. For instance, studies conducted by Zhou *et al.* [14] and Yoo *et al.* [35] could be used by enriching their modeling with finer results to get rid of data fitting. DNS results such as those regarding bubble growth in a flowing superheated or subcooled liquid by Legendre *et al.* [49] could be of interest in that prospect.

Finally, the precise estimation of the contact angle and hysteresis remains a critical parameter to predict departure by sliding as demonstrated throughout this study. Local measurements of those values and their evolution with operating conditions would be a very valuable information in that regard. The article of Song & Fan [45] that sums up existing modeling and experimental measurements provides a good overview of the problem and identifies the associated challenges that are still to be tackled.

6. Acknowledgements

This work was funded by Électricité de France (EDF) in collaboration with Institut de Mécanique des Fluides de Toulouse (IMFT).

7. References

References

[1] A. Guelfi, D. Bestion, M. Boucker, P. Boudier, P. Fillion, M. Grandotto, J.-M. Hérard, E. Hervieu, P. Péturaud, NEPTUNE: A New Software Platform for

Advanced Nuclear Thermal Hydraulics, Nuclear Science and Engineering 156 (2007) 281–324. doi:10.13182/NSE05-98.

[2] N. Kurul, M. Z. Podowski, Multidimensional Effects In Forced Convection Subcooled Boiling, Begel House Inc., 1990. doi:10.1615/IHTC9.40.

[3] N. Basu, G. R. Warrier, V. K. Dhir, Wall Heat Flux Partitioning During Subcooled Flow Boiling: Part 1–Model Development, Journal of Heat Transfer 127 (2005) 131–140. doi:10.1115/1.1842784.

[4] L. Gilman, E. Baglietto, A self-consistent, physics-based boiling heat transfer modeling framework for use in computational fluid dynamics, International Journal of Multiphase Flow 95 (2017) 35–53. doi:10.1016/j.ijmultiphaseflow.2017.04.018.

[5] J. Bhati, S. Paruya, J. Naik L., Numerical simulation of bubble dynamics in subcooled flow boiling in a channel, Nuclear Engineering and Design 371 (2021) 110945. doi:https://doi.org/10.1016/j.nucengdes.2020.110945.

[6] R. Situ, T. Hibiki, M. Ishii, M. Mori, Bubble lift-off size in forced convective subcooled boiling flow, International Journal of Heat and Mass Transfer 48 (2005) 5536–5548. doi:10.1016/j.ijheatmasstransfer.2005.06.031.

[7] S. Maity, Effect of Velocity and Gravity on Bubble Dynamics, Master's thesis, University of California Los Angeles, 2000.

[8] Y. Rousselet, G. Warrier, V. K. Dhir, Experimental study of bubble dynamics during nucleate flow boiling on horizontal and vertical surfaces, Journal of Enhanced Heat Transfer 21:4-5 (2014) 259–282. doi:10.1615/JEnhHeatTransf.2015013429.

[9] A. Kossolapov, Experimental Investigation of Subcooled Flow Boiling and CHF at Prototypical Pressures of Light Water Reactors, PhD Thesis, Massachusetts Institute of Technology, 2021.

[10] C. E. Estrada-Pérez, Y. A. Hassan, B. Alkhudhiri, J. Yoo, Time-resolved measurements of liquid-vapor thermal interactions throughout the full life-cycle of sliding bubbles at subcooled flow boiling conditions, International Journal of Multiphase Flow 99 (2018) 94–110. doi:10.1016/j.ijmultiphaseflow.2017.10.002.

[11] A. Richenderfer, A. Kossolapov, J. H. Seong, G. Saccone, E. Demarly, R. Kommajosyula, E. Baglietto, J. Buongiorno, M. Bucci, Investigation of subcooled flow boiling and CHF using high-resolution diagnostics, Experimental Thermal and Fluid Science 99 (2018) 35–58. doi:10.1016/j.expthermflusci.2018.07.017.

[12] H. C. Unal, Maximum bubble diameter, maximum bubble-growth time and bubble-growth rate during the subcooled nucleate flow boiling of water up to 17.7 MN/m2, International Journal of Heat and Mass Transfer 19 (1976) 643–649. doi:10.1016/0017-9310(76)90047-8.

[13] J. F. Klausner, R. Mei, D. M. Bernhard, L. Z. Zeng, Vapor bubble departure in forced convection boiling, International Journal of Heat and Mass Transfer 36 (1993) 651–662. doi:10.1016/0017-9310(93)80041-R.

[14] P. Zhou, R. Huang, S. Huang, Y. Zhang, X. Rao, Experimental investigation on bubble contact diameter and bubble departure diameter in horizontal subcooled flow boiling, International Journal of Heat and Mass Transfer 149 (2020) 119105. doi:10.1016/j.ijheatmasstransfer.2019.119105.

[15] W. G. J. Van Helden, C. W. M. Van Der Geld, P. G. M. Boot, Forces on bubbles growing and detaching in flow along a vertical wall, International Journal of Heat and Mass Transfer 38 (1995) 2075–2088. doi:10.1016/0017-9310(94)00319-Q.

[16] G. Thorncroft, J. Klausner, R. Mei, Bubble forces and detachment models, Multiphase Science and Technology 13 (2001) 35–76. doi:10.1615/multscientechn.v13.i3-4.20.

[17] G. Duhar, C. Colin, Dynamics of bubble growth and detachment in a viscous shear flow, Physics of Fluids 18 (2006) 077101. doi:10.1063/1.2213638.

[18] R. Sugrue, J. Buongiorno, T. McKrell, An experimental study of bubble departure diameter in subcooled flow boiling including the effects of orientation angle, subcooling, mass flux, heat flux, and pressure, Nuclear Engineering and Design 279 (2014) 182–188. doi:10.1016/j.nucengdes.2014.08.009.

[19] T. Mazzocco, W. Ambrosini, R. Kommajosyula, E. Baglietto, A reassessed model for mechanistic prediction of bubble departure and lift off diameters, International Journal of Heat and Mass Transfer 117 (2018) 119–124. doi:10.1016/j.ijheatmasstransfer.2017.09.105.

[20] T. Ren, Z. Zhu, R. Zhang, J. Shi, C. Yan, Development of force balance model for prediction of bubble departure diameter and lift-off diameter in subcooled flow boiling, International Journal of Heat and Mass Transfer 161 (2020) 120245. doi:10.1016/j.ijheatmasstransfer.2020.120245.

[21] J. Bhati, S. Paruya, Numerical simulation of bubble dynamics in pool boiling at heated surface, International Journal of Heat and Mass Transfer 152 (2020) 119465. doi:https://doi.org/10.1016/j.ijheatmasstransfer.2020.119465.

[22] L. Bures, Y. Sato, On the modelling of the transition between contact-line and microlayer evaporation regimes in nucleate boiling, Journal of Fluid Mechanics 916 (2021). doi:10.1017/jfm.2021.204.

[23] R. Sugrue, J. Buongiorno, A modified force-balance model for prediction of bubble departure diameter in subcooled flow boiling, Nuclear Engineering and Design 305 (2016) 717–722. doi:10.1016/j.nucengdes.2016.04.017.

[24] R. Mei, J. F. Klausner, Unsteady force on a spherical bubble at finite Reynolds number with small fluctuations in the free-stream velocity, Physics of Fluids A: Fluid Dynamics 4 (1992) 63–70. doi:10.1063/1.858501.

[25] D. Legendre, J. Magnaudet, The lift force on a spherical bubble in a viscous linear shear flow, Journal of Fluid Mechanics 368 (1998) 81–126. doi:10.1017/S0022112098001621.

[26] L. Zeng, F. Najjar, S. Balachandar, P. Fischer, Forces on a finite-sized particle located close to a wall in a linear shear flow, Physics of Fluids 21 (2009) 033302. doi:10.1063/1.3082232.

[27] P. Shi, R. Rzehak, D. Lucas, J. Magnaudet, Drag and lift forces on a rigid sphere immersed in a wall-bounded linear shear flow, Physical Review Fluids 6 (2021) 104309.

[28] V. Scheiff, F. Bergame, J. Sebilleau, P. Ruyer, C. Colin, Experimental study of steady and transient subcooled flow boiling, International Journal of Heat and Mass Transfer 164 (2021) 120548. doi:10.1016/j.ijheatmasstransfer.2020.120548.

[29] J. Magnaudet, I. Eames, The Motion of High-Reynolds-Number Bubbles in Inhomogeneous Flows, Annual Review of Fluid Mechanics 32 (2000) 659–708. doi:10.1146/annurev.fluid.32.1.659.

[30] P. Guan, L. Jia, L. Yin, Z. Tan, Bubble departure size in flow boiling, Heat and Mass Transfer 51 (2015) 921–930. doi:10.1007/s00231-014-1461-7.

[31] S. H. Lamb, Hydrodynamics, University Press, 1895.

[32] L. V. Wijngaarden, D. J. Jeffrey, Hydrodynamic interaction between gas bubbles in liquid, Journal of Fluid Mechanics 77 (1976) 27–44. doi:10.1017/S0022112076001110.

[33] C. W. M. van der Geld, The dynamics of a boiling bubble before and after detachment, Heat and Mass Transfer 45 (2009) 831–846. doi:10.1007/s00231-007-0254-7.

[34] D. Legendre, C. Colin, T. Coquard, Lift, drag and added mass of a hemispherical bubble sliding and growing on a wall in a viscous linear shear flow, Philosophical Transactions of the Royal Society A: Mathematical, Physical and Engineering Sciences 366 (2008) 2233–2248. doi:10.1098/rsta.2008.0009.

[35] J. Yoo, C. E. Estrada-Perez, Y. A. Hassan, Development of a mechanistic model for sliding bubbles growth prediction in subcooled boiling flow, Applied Thermal Engineering 138 (2018) 657–667. doi:10.1016/j.applthermaleng.2018.04.096.

[36] O. Levenspiel, Collapse of Steam Bubbles in Water, Industrial & Engineering Chemistry 51 (1959) 787–790. doi:10.1021/ie50594a045.

[37] A. Urbano, S. Tanguy, G. Huber, C. Colin, Direct numerical simulation of nucleate boiling in micro-layer regime, International Journal of Heat and Mass Transfer 123 (2018) 1128–1137. doi:10.1016/j.ijheatmasstransfer.2018.02.104.

[38] M. S. Plesset, S. A. Zwick, The Growth of Vapor Bubbles in Superheated Liquids, Journal of Applied Physics 25 (1954) 493–450.

[39] H. K. Forster, N. Zuber, Growth of a Vapor Bubble in a Superheated Liquid, Journal of Applied Physics 25 (1954) 474–478. doi:10.1063/1.1721664.

[40] N. Zuber, The dynamics of vapor bubbles in nonuniform temperature fields, International Journal of Heat and Mass Transfer 2 (1961) 83–98. doi:10.1016/0017-9310(61)90016-3.

[41] H. Reichardt, Vollstandige Darstellung der turbulenten Geschwindigkeitsverteilung in glatten Leitungen, Zeitschrift Angewandte Mathematik und Mechanik 31 (1951) 208–219. doi:10.1002/zamm.19510310704.

[42] W. H. McAdams, Heat transmission, McGraw-Hill, New York, 1954.

[43] G. Kocamustafaogullari, Pressure dependence of bubble departure diameter for water, International Communications in Heat and Mass Transfer 10 (1983) 501–509. doi:10.1016/0735-1933(83)90057-X.

[44] W. Frost, G. S. Dzakowic, American Society of Mechanical Engineers, An extension of the method for predicting incipient boiling on commercially finished surfaces, ASME, New York, N.Y., 1967.

[45] J.-W. Song, L.-W. Fan, Temperature dependence of the contact angle of water: A review of research progress, theoretical understanding, and implications for boiling heat transfer, Advances in Colloid and Interface Science 288 (2021) 102339. doi:10.1016/j.cis.2020.102339.

[46] S. G. Kandlikar, M. E. Steinke, Contact angles and interface behavior during rapid evaporation of liquid on a heated surface, International Journal of Heat and Mass Transfer 45 (2002) 3771–3780. doi:10.1016/S0017-9310(02)00090-X.

[47] M. Bucci, J. Buongiorno, M. Bucci, The not-so-subtle flaws of the force balance approach to predict the departure of bubbles in boiling heat transfer, Physics of Fluids 33 (2021) 017110. doi:10.1063/5.0036956.

[48] G. E. Thorncroft, J. F. Klausner, R. Mei, An experimental investigation of bubble growth and detachment in vertical upflow and downflow boiling, International Journal of Heat and Mass Transfer 41 (1998) 3857–3871. doi:10.1016/S0017-9310(98)00092-1.

[49] D. Legendre, J. Borée, J. Magnaudet, Thermal and dynamic evolution of a spherical bubble moving steadily in a superheated or subcooled liquid, Physics of Fluids 10 (1998) 1256–1272. doi:10.1063/1.869654.

[50] J. Garnier, E. Manon, G. Cubizolles, Local Measurements On Flow Boiling Of Refrigerant 12 In A Vertical Tube, Multiphase Science and Technology 13 (2001). doi:10.1615/MultScienTechn.v13.i1-2.10.

[51] D. Chen, L.-m. Pan, S. Ren, Prediction of bubble detachment diameter in flow boiling based on force analysis, Nuclear Engineering and Design 243 (2012) 263–271. doi:10.1016/j.nucengdes.2011.11.022.